Unraveling the Role of Ctla-4 in Intestinal Immune Homeostasis: Insights from a novel Zebrafish Model of Inflammatory Bowel Disease

Lulu Qin[a], Chongbin Hu[a], Qiong Zhao[a], Yong Wang[a], Dongdong Fan[a], Aifu Lin[a], Lixin Xiang[a*], Ye Chen[a,c*], Jianzhong Shao[a,b*]

Affiliations:

[a]College of Life Sciences, Key Laboratory for Cell and Gene Engineering of Zhejiang Province, Zhejiang University, Hangzhou, China.

[b]Laboratory for Marine Biology and Biotechnology, Qingdao National Laboratory for Marine Science and Technology, Qingdao, China

[c]Department of Genetic and Metabolic Disease, the Children's Hospital, Zhejiang University School of Medicine, National Clinical Research Center for Child Health, Hangzhou 310052, China.

[*]Corresponding authors: shaojz@zju.edu.cn, yechency@zju.edu.cn, and xianglx@zju.edu.cn

Address correspondence and reprint requests to Prof. Jianzhong Shao, Prof. Ye Chen, and Assoc. Prof. Lixin Xiang, College of Life Sciences, Zhejiang University, 866 YuHangTang Road, Hangzhou 310058, China. Tel.: +86 (571) 88206582; Fax: +86 (571) 88206582.

E-mail addresses: shaojz@zju.edu.cn (J.-z.S.), yechency@zju.edu.cn (Y.C), and xianglx@zju.edu.cn (L.-x.X.)

Abstract

Inflammatory bowel disease (IBD) is a chronic and relapsing immune-mediated disorder characterized by intestinal inflammation and epithelial injury. The underlying causes of IBD are not fully understood, but genetic factors have implicated in genome-wide association studies, including CTLA-4, an essential negative regulator of T cell activation. However, establishing a direct link between CTLA-4 and IBD has been challenging due to the early lethality of CTLA-4 knockout mice. In this study, we identified zebrafish Ctla-4 homolog and investigated its role in maintaining intestinal immune homeostasis by generating a Ctla-4-deficient (*ctla-4*$^{-/-}$) zebrafish line. These mutant zebrafish exhibit reduced weight, along with impaired epithelial barrier integrity and lymphocytic infiltration in their intestines. Transcriptomics analysis revealed upregulation of inflammation-related genes, disturbing immune system homeostasis. Moreover, single-cell RNA-sequencing analysis indicated increased Th2 cells and interleukin 13 expression, along with decreased innate lymphoid cells and upregulated proinflammatory cytokines. Additionally, Ctla-4-deficient zebrafish exhibited reduced diversity and an altered composition of the intestinal microbiota. All these phenotypes closely resemble those found in mammalian IBD. Lastly, supplementation with Ctla-4-Ig successfully alleviated intestinal inflammation in these mutants. Altogether, our findings demonstrate the pivotal role of Ctla-4 in maintaining intestinal homeostasis. Additionally, they offer substantial evidence linking CTLA-4 to IBD and establish a novel zebrafish model for investigating both the pathogenesis and potential treatments.

Key words: Ctla-4 deficiency; inflammatory bowel disease; molecular and cellular mechanisms; zebrafish model

Introduction

Inflammatory bowel disease (IBD), including Crohn's disease and ulcerative colitis, refers to a group of chronic relapsing inflammation disorders affecting the gastrointestinal tract, that have been increasing in prevalence worldwide [1]. The precise etiology of IBD has yet to be fully elucidated. Conventional epidemiological studies have indicated that IBD tends to run in families and is linked to genetic factors [2, 3]. However, research also suggested that susceptibility gene patterns differ significantly among various geographic populations. Current evidence points towards a complicated interaction involving host genetics, disrupted intestinal microbiota, environmental triggers, and abnormal immune responses [4-6]. Advances in genomic sequencing techniques have allowed for the identification of genetic variants associated with an increased risk of developing IBD. Among these, mutations in immune-related genes have received particular attention. Research on humans with Crohn's disease and mouse models of IBD has shown that genetically susceptible individuals exhibit defects in intracellular pattern-recognition receptors (PRRS), such as toll-like receptors (TLR) and nucleotide-binding oligomerization domain (NOD)-like receptors (NLRs), which are responsible for initiating innate immune responses to eliminate harmful bacteria [7, 8]. Genetic variations in the tumor necrosis factor ligand superfamily member 15 (TNFSF15) and interleukin 23 receptor (IL23R) genes, both involved in suppressing

66 inflammation, have been associated with an increased risk of developing Crohn's
67 disease [9, 10].

68 Cytotoxic T-cell associated antigen-4 (CTLA-4), also known as CD152, is one of
69 the most well-established immune checkpoint molecules expressed predominantly on
70 T cells. It primarily regulates the early stages of T-cell activation by attenuating
71 downstream signaling of the T cell receptor (TCR) [11-13]. Specifically, CTLA-4 has
72 a much higher affinity for CD80 and CD86 ligands compared to the co-stimulatory
73 receptor CD28 [14, 15]. By outcompeting CD28 for ligand binding, CTLA-4 provides
74 an inhibitory signal that impacts immunological synapse formation and inhibits T-cell
75 proliferation and activation [13, 16]. As expected, links between polymorphic alleles of
76 CTLA4 and IBD have been reported in multiple studies [17-19]. Moreover, CTLA-4 is
77 an intriguing target for novel immune checkpoint blockade therapies in cancer
78 treatment, while intestinal inflammation is a common side effect in these clinical trials
79 [20, 21]. Establishing a direct causal relationship between CTLA-4 and IBD has been
80 challenging due to difficulties in finding appropriate models. Early lethality was
81 observed in CTLA-4-deficient mice, adding to the complexity of this issue. Zebrafish
82 is a powerful model system for immunological and biomedical research, due to its
83 versatility and high degree of conservation in innate and adaptive immunities. In our
84 current study, we identified the Ctla-4 homology in zebrafish and successfully
85 developed an adult vertebrate model with homozygous knockout of the *ctla-4* gene for
86 the first time. These *ctla-4*-deficient (*ctla-4*$^{-/-}$) zebrafish survive but exhibit attenuated
87 growth and weight loss. Notably, *ctla-4* deficiency leads to an IBD-like phenotype in

88 zebrafish characterized by altered intestinal epithelial cells morphology, abnormal
89 inflammatory response, defects in microbial stratification and composition.
90 Mechanistically, Ctla-4 exerts its inhibitory function by competing with Cd28 for
91 binding to Cd80/86. These findings establish the *ctla-4* knockout zebrafish as an
92 innovative platform to elucidate CTLA-4 immunobiology, model human IBD, and
93 develop novel therapeutic modalities.
94

95 ## Results

96 **Identification of zebrafish Ctla-4**

97 Through a homology search in the NCBI database, we identified the *ctla-4* gene
98 on zebrafish chromosome 9 (Fig. S1A-C). Zebrafish Ctla-4 protein contains an N-
99 terminal signal peptide, a single IgV-like extracellular domain, a transmembrane region,
100 and a cytoplasmic tail (Fig. 1A). A ^{113}LFPPPY^{118} motif is present in the ectodomain of
101 Ctla-4, similar to the MYPPPY motif, a binding site for CD80/CD86 found in mammals
102 (Fig. 1A). Thus, we reasoned that the ^{13}LFPPPY^{118} motif may be a potential binding
103 site for Cd80/86 in zebrafish. The tyrosine-based YVKM motif in the cytoplasmic
104 domain in mammals, which is involved in internalization and signaling inhibition, is
105 absent in Ctla-4. By contrast, a unique tyrosine-based ^{206}YVKF^{209} motif was found in
106 the C-terminus of Ctla-4 molecule, which is relatively conserved in different fish
107 species (Fig. 1A). The IgV-like domain of Ctla-4 was characterized by two-layer β-
108 sandwich and was conserved between zebrafish and humans (Fig. 1B). Ctla-4 exists as
109 a dimer, and unlike the intracellular localization of CTLA-4 in mammals, Ctla-4 was

located on the cell membrane (Fig. 1C and D). Moreover, Ctla-4 was mainly expressed on the T cells, including the $Cd4^+$ T cells and $Cd8^+$ T cells (Fig. 1E and F).

Ctla-4 deficiency induces inflammatory bowel disease (IBD)-like phenotype

To further investigate the function of Ctla-4, we generated a *ctla-4*$^{-/-}$ zebrafish line with a 14-base deletion in the second exon of the *ctla-4* gene (Fig. 2A-C). The zebrafish appeared grossly normal in appearance; however, the body weight and size were significantly reduced compared with those of wild-type zebrafish (Fig. 2D and E). Anatomically, the *ctla-4*$^{-/-}$ zebrafish were featured by intestine shortening and splenomegaly, suggesting the occurrence of chronic inflammation in the intestines (Fig. 2F and G). For clarification, we first performed histological analysis on the anterior, mid, and posterior intestine segments using H&E staining. Compared with the wild-type zebrafish, the *ctla-4*$^{-/-}$ fish exhibited significant epithelial hyperplasia in the anterior intestine segment, accompanied with a small amount of mucosal inflammatory cell infiltration (Fig. 2H). This result indicates an enhanced regeneration of the intestine, which is typically observed in cases of intestinal inflammation [22]. A noteworthy goblet cell loss which marks the severity of intestinal inflammation was also observed in *ctla-4*$^{-/-}$ anterior intestine, as quantified through PAS staining (Fig. 2I and J). Besides, a small amount of lymphocytic infiltration and mild epithelial damage occurred in the mid intestine segment of *ctla-4*$^{-/-}$ zebrafish (Fig. 2H). In posterior intestine of *ctla-4*$^{-/-}$ fish, the intestinal villi were markedly shortened, the epithelial barrier showed severely disrupted, and the intestinal wall became thinner, wherein the mucosal and transmural inflammatory cells were significantly infiltrated (Fig. 2H). Consistent with these

132 observations, ultrastructure analysis revealed that the epithelial cells of posterior
133 intestine in *ctla-4*$^{-/-}$ zebrafish exhibited alteration in tight junction, the loss of adhesion
134 junctions and desmosomes, and disruption of microvilli (Fig. 2K). All these results
135 strongly indicate that Ctla-4 plays a crucial role in preserving intestinal homeostasis in
136 zebrafish. The intestinal phenotype resulting from Ctla-4 deficiency was similar to IBD
137 in mammals.

138 **Molecular mechanisms of Ctla-4 deficiency-induced IBD-like phenotype**

139 To explore the potential molecular mechanisms of Ctla-4 deficiency-induced IBD-
140 like phenotype, we performed transcriptome profiling analysis of intestines from wild-
141 type and *ctla-4*$^{-/-}$ zebrafish. We identified a total of 1,140 differentially expressed genes
142 (DEGs), among which 714 genes were up-regulated, and 426 genes were down-
143 regulated in *ctla-4*$^{-/-}$ zebrafish (Fig. 3A and B). GO enrichment analysis showed that
144 DEGs or up-regulated genes in the top 10 enriched biological processes were associated
145 with the immune response and inflammatory response (Fig. 3C and D). Moreover, the
146 KEGG enrichment analyses indicated that the up-regulated DEGs are primarily
147 involved in the process of cytokine-cytokine receptor interaction and cell adhesion
148 molecules, which are also related to inflammation (Fig. S3A); however, the down-
149 regulated DEGs were significantly enriched in the process of metabolism (Fig. S3B).
150 The intestines of *ctla-4*$^{-/-}$ zebrafish showed significant upregulation of *il1b*, *tnfa*,
151 myeloid-specific peroxidase (*mpx*), matrix metallopeptidase 9 (*mmp9*), chemokine (C-
152 X-C motif) ligand 8a (*cxcl8a*), and *il13*, a Th2-typic cytokine crucial for ulcerative
153 colitis in mammals [23]. In contrast, *il10*, a potent anti-inflammatory cytokine, was

154 markedly down-regulated in Ctla-4-deficient intestines (Fig. 3E). The transcriptional
155 change of these genes was confirmed by RT-qPCR (Fig. 3F). By constructing the PPI
156 network, we found that *il1b* was a major cytokine that played a hub role in promoting
157 the bowel inflammation of *ctla-4*$^{-/-}$ zebrafish (Fig. 3G). Moreover, Gene set enrichment
158 analysis (GSEA) showed that genes involved in the lymphocyte chemotaxis, positive
159 regulation of ERK1 and ERK2 cascade, Calcium and MAPK signaling pathways were
160 positively enriched in *ctla-4*$^{-/-}$ zebrafish intestines, implying a sensitized or activated
161 state of lymphocytes due to the absence of Ctla-4 (Fig. S3C and D). Notably, biological
162 processes related to neutrophil activation and chemotaxis were significantly enriched
163 (Fig. 3C and D). Studies have shown that neutrophils can induce histopathological
164 effects through releasing matrix metalloproteinases (MMPs), neutrophil elastase, and
165 myeloperoxidase (MPO) [24]. To confirm the association between neutrophils and Ctla-
166 4-deficient intestinal inflammation, the MPO level was examined. As a support, MPO
167 activity was markedly increased in the intestines and peripheral blood of *ctla-4*$^{-/-}$
168 zebrafish (Fig. 3H). Besides, a number of biological markers or susceptibility genes of
169 IBD observed in mammals, including c-reactive protein 6 (*crp6*), *crp7*, MMPs,
170 haptoglobin, *il23r*, insulin-like growth factor binding protein 1 a (*igfbp1a*), cAMP
171 responsive element modulator b (*cremb*) and lymphocyte specific protein 1 b (*lsp1b*),
172 were highly expressed in the *ctla-4*$^{-/-}$ zebrafish (Fig. 3I and J) [9, 25, 26], suggesting the
173 presence of a conserved molecular network underlying IBD pathogenesis between *ctla-*
174 *4*$^{-/-}$ zebrafish and mammalian models.

175 **Cellular mechanisms of Ctla-4 deficiency-induced IBD-like phenotype**

To investigate the cellular mechanisms underlying the IBD-like phenotype induced by Ctla-4 deficiency, we performed scRNA-seq analysis on intestines from wild-type and *ctla-4*$^{-/-}$ zebrafish using the 10× Genomics Chromium platform. We obtained nine discrete clusters from 7,539 cells of wild-type and *ctla-4*$^{-/-}$ zebrafish (Fig. 4A). These clusters of cells were classified as enterocytes, enteroendocrine cells, smooth muscle cells, neutrophils, macrophages, B cells, and a group of T/NK/ILC-like cells based on their co-expression of lineage marker genes (Fig. 4B and C, Fig. S4A and B). Due to severe epithelial disruption and inflammatory cell infiltration in *ctla-4*$^{-/-}$ zebrafish intestines, we focus on the pathological process and immune reactions in enterocytes and immune cell populations. KEGG analysis showed that apoptotic pathway was highly enriched in enterocytes of *ctla4*$^{-/-}$ zebrafish, suggesting that aberrant apoptosis contributes to the epithelial injury (Fig. S4C). Additionally, genes functionally involved in the formation of tight and adhesion junctions, such as *oclna*, *cdh1*, *pcdh1b* and *cldn15a*, were significantly down-regulated in enterocytes of *ctla-4*$^{-/-}$ zebrafish (Fig. 4D), consistent with the pathological observation under electron microscope. Furthermore, inflammation-related genes and pathways were significantly up-regulated and enriched in neutrophils, B cells, and macrophages of *ctla-4*$^{-/-}$ zebrafish, suggesting active inflammatory responses (Fig. 4E-G, Fig. S4D). By sub-clustering analysis, six subpopulations were classified from T/NK/ILC-like cell groups based on their expression with a set of marker genes. These subpopulations include Cd8^{+} T cells, ILC3-like cells, maturing Ccr7^{high} T cells, NKT cells, and two groups of Th2 cells (Fig. 5A-C; Fig. S5A). The abundances of NKT and two subsets of Th2 cells were

198 significantly increased in the intestines of *ctla-4*$^{-/-}$ zebrafish (Fig. 5D-F). These cells
199 exhibited high expression of *il13*, a key contributor to intestinal inflammation in
200 mammals (Fig. 5G and H) [23]. Specifically, the second subset of Th2 cells was seldom
201 observed in the intestine of wild-type zebrafish, indicating their unique role in the
202 pathogenesis of IBD-like phenotype in *ctla-4*$^{-/-}$ zebrafish (Fig. 5D-F). KEGG analysis
203 of up-regulated genes from *ctla-4*$^{-/-}$ NKT and Th2 cells indicated that Ctla-4 deficiency
204 is positively associated with the inflammatory cytokine-cytokine receptor interaction,
205 PPAR, calcium and MAPK signaling pathways, cellular adhesion and mucosal immune
206 responses (Fig. 5I and J; Fig. S5B), suggesting high activity of NKT and Th2 cells in
207 inflamed intestines [27, 28]. Although the abundance of Cd8^{+} T cells was not
208 significantly changed in Ctla-4-deficient intestines, the inflammatory genes and
209 pathways were up-regulated and enriched in the subset of T cells (Fig. S5C and D).
210 Notably, the proportion of ILC3-like cells was decreased, and they highly expressed
211 *il17a/f1* and *il17a/f3* in the Ctla-4-deficient intestines (Fig. 5D-F, and K). Investigations
212 have consistently reported a substantial decline in the population of ILC3s within the
213 inflamed intestines and IL-17A-secreting ILC3s play a significant role in the
214 development of intestinal inflammation [29-34]. Thus, the reduced ILC3-like cells and
215 increased expression of *il17a/f1* and *il17a/f3* may be responsible for intestinal
216 inflammation induced by Ctla-4 deficiency.

217 **Decreased microbiota diversity in *ctla-4*$^{-/-}$ zebrafish intestines**

218 The intestinal microbiota plays a crucial role in host functions such as nutrient
219 acquisition, metabolism, epithelial cell development and immunity. Notably, lower

220 microbiota diversity has consistently been observed in patients with IBD phenotype [35,
221 36], making it a valuable indicator of host health. Therefore, we further analyzed
222 whether microbes are involved in the Ctla-4-deficiency induced intestinal inflammation.
223 The results revealed a significantly higher number of amplicon sequence variants
224 (ASVs) in wild-type zebrafish intestines, with 730 ASVs unique to the wild-type group
225 and 276 ASVs exclusively found in *ctla-4*$^{-/-}$ group (Fig. 6A). Furthermore, the Shannon
226 index and the Simpson index indicated a decreased microbial diversity in *ctla-4*$^{-/-}$
227 zebrafish intestines (Fig. 6B) and the Principal Coordinate Analysis (PCoA) using Bray
228 Curtis distance revealed a significant separation in the microbial composition between
229 *ctla-4*$^{-/-}$ group and the wild-type group (Fig. 6C). To gain insights into the microbial
230 community composition, we analyzed the identified microbial populations at the class
231 and family level. Alphaproteobacteria and Gammaproteobacteria were found to be the
232 most prevalent classes. Relative to wild-type group, Ctla-4 deficiency resulted in a
233 significant reduction in Alphaproteobacteria abundance. However, the
234 Gammaproteobacteria, one of the main classes of Gamma-negative pathogenic bacteria
235 expanded under inflammation conditions, was increased, although the change did not
236 reach statistical significance (Fig. 6D and E) [37]. In addition, we observed a decreased
237 relative abundance of short-chain fatty acids (SCFAs)-producing Bacilli and
238 Verrucomicrobiae, the latter of which contributes to glucose homeostasis and intestinal
239 health (Fig. 6F and G) [38, 39]. Notably, the family-level analysis revealed a notable
240 enrichment of Enterobacteriaceae, overgrowing under host inflammatory conditions,
241 and the Shewanellaceae, serving as the most important secondary or opportunistic

242 pathogens, in *ctla-4*$^{-/-}$ zebrafish (Fig. 6H and I). To identify differentially abundant
243 bacterial taxa between the wild-type and *ctla-4*$^{-/-}$ zebrafish, we conducted Linear
244 discriminant analysis (LDA) effect size (LEfSe). The results showed that several
245 potentially opportunistic pathogens, including Gammaproteobacteria, Enterobacterales,
246 and Aeromonadales were found to be overrepresented in *ctla-4*$^{-/-}$ zebrafish (Fig. 6J). In
247 contrast, Actinobacteriota, Cetobacterium, and Planctomycetota (Planctomycetes) were
248 more abundant in the wild-type zebrafish. These findings strongly indicated an
249 association between Ctla-4 deficiency-induced gut inflammation and dysbiosis, as
250 characterized by decreased microbial diversity, loss of potentially beneficial bacteria,
251 and expansion of pathobionts.

252 **Inhibitory role of Ctla-4 in T cell activation**

253 Given that Ctla-4 is primarily expressed on T cells (Fig. 1E-F), and its absence has
254 been shown to result in intestinal immune dysregulation, indicating a crucial role of this
255 molecule as a conserved immune checkpoint in T cell inhibition. For clarification, the
256 lymphocyte proliferation was examined by a series of blockade/inhibition assays using
257 anti-Ctla-4 Ab, recombinant soluble Ctla-4-Ig (sCtla-4-Ig), sCd28-Ig, and sCd80/86
258 proteins in a PHA-stimulating and mixed lymphocyte reaction (MLR) model (Fig. S6
259 A-C). Results showed that the lymphocyte proliferation was more pronounced in the
260 absence of Ctla-4, and the supplementation of sCtla-4-Ig inhibited cell proliferation,
261 suggesting the inhibitory function of Ctla-4 in T cells (Fig. 7A and B). Consistent with
262 these results, blockade of Ctla-4 by administering anti-Ctla-4 Ab significantly promoted
263 the proliferation of lymphocytes from wild-type zebrafish (Fig. 7C). Moreover,

264 administration of sCd28-Ig into the co-cultures also inhibited the proliferation of
265 lymphocytes from *ctla-4*$^{-/-}$ zebrafish (Fig. 7D). Besides, the addition of Cd80/86
266 significantly promoted the expansion of Ctla-4-deficient lymphocytes (Fig. 7E). Based
267 on these results, we concluded that the presence of Ctla-4 obstructs the Cd80/86-Cd28
268 mediated costimulatory signaling, consequently impeding cell proliferation. To further
269 investigate the relationship between Cd28, Ctla-4 and Cd80/86, we assessed the
270 interaction between these molecules *in vitro*. Our bioinformatics analysis by
271 AlphaFold2, flow cytometry and Co-IP assays demonstrated the interaction between
272 Cd28/Ctla-4 and Cd80/86 (Fig. 7F-H, Fig. S6D). Moreover, using a microscale
273 thermophoresis assay, we found that Ctla-4 has higher affinity for Cd80/86 than Cd28,
274 as indicated by a lower equilibrium association constant value (K_D = 0.50 ± 0.25 μM
275 vs. K_D = 2.64 ± 0.45 μM) (Fig. 7I). These results suggested that Ctla-4 could exert its
276 inhibitory function by competing with Cd28 for binding Cd80/86.

277 **sCtla-4-Ig alleviates IBD-like phenotype**

278 As described above, engagement of Cd80/86 by sCtla-4-Ig effectively suppressed
279 T cell activation *in vitro* (Fig. 7B), indicating that sCtla-4-Ig holds promise as a
280 potential intervention for IBD-like phenotype. This is supported by the observation that
281 zebrafish treated with sCtla-4-Ig exhibited obvious body weight restoration compared
282 to those treated with the IgG isotype control (Fig. 8A). To provide further evidence,
283 histological analysis was performed on the posterior intestine, which is known to
284 experience severe tissue destruction under Ctla-4 deficient conditions. As expected,
285 Ctla-4-Ig treatment resulted in a significant decrease in lymphocyte infiltration and an

286 improvement in the epithelial barrier (Fig. 8B). Moreover, Ctla-4-Ig treatment
287 significantly reduced the expression of pro-inflammatory genes, including *il13*, *tnfa*,
288 *mpx*, *mmp9*, and *cxcl8a*, as well as *igfbp1a*, *cremb*, and *lsp1a*, which are susceptibility
289 genes for IBD observed in mammals (Fig. 8C and D). These findings demonstrate that
290 the supplementation of Ctla-4-Ig alleviates intestinal inflammation in Ctla-4-deficient
291 zebrafish, highlighting its potential as a therapeutic intervention for CTLA-4
292 deficiency-induced IBD in mammals.
293

294 **Discussion**

295 As an essential negative regulator of T cell activation, dysfunction of CTLA-4 was
296 implicated in various diseases in both humans and murine models [40-42]. Numerous
297 previous studies have established the connection between CTLA-4 and autoimmune
298 thyroiditis, Graves' disease, myocarditis, pancreatitis, multiple sclerosis, rheumatoid
299 arthritis, and type I diabetes [43-49]. However, the involvement of CTLA-4 in IBD has
300 been understudied. Several investigations have reported that haploinsufficiency
301 resulting from mutations in CTLA-4 in humans is associated with IBD, and genome-
302 wide association studies (GWAS) have implicated CTLA-4 as a susceptibility gene for
303 IBD [50-52]. Nevertheless, the exact contributions and mechanisms of CTLA-4
304 deficiency in the occurrence and pathology of IBD remain incompletely understood,
305 primarily due to the lack of animal models attributable to the lethality of CTLA-4
306 knockout in mice. In this study, we identified the Ctla-4 homolog in zebrafish, and
307 discovered that defect in Ctla-4 did not have a severe lethal effect, but did show a clear

308 IBD-like phenotype. This makes zebrafish an attractive animal model for investigating
309 the molecular and cellular mechanisms underlying Ctla-4 mediated IBD. Multiple lines
310 of experimental evidence demonstrated the IBD-like phenotype in Ctla-4-deficienct
311 zebrafish. These include the observed destruction of epithelial integrity and infiltration
312 of inflammatory cells in the inflamed intestines during histopathological analysis, the
313 enrichment of inflammation-related pathways and the imbalance between pro-
314 inflammatory and anti-inflammatory cytokines identified through transcriptome
315 profiling, the abnormal composition of immune cell populations revealed by single-cell
316 RNA sequencing, as well as the reduced diversity and altered composition of intestinal
317 microbiota. These observations collectively suggest that Ctla-4 may serve as a potential
318 genetic determinant of the IBD-like phenotype, although further research is required to
319 definitively identify the causative variant responsible for this association. Moreover,
320 the establishment of zebrafish models provides a valuable tool for comprehending the
321 underlying mechanisms of the disease's pathophysiology.

322 A multi-omics study was conducted to investigate the mechanisms of Ctla-4-
323 deficiency induced IBD. RNA-seq analysis demonstrated a significant upregulation of
324 important inflammatory cytokines, such as *il1b* and *tnfa* in the Ctla-4-deficient
325 intestines. This is consistent with studies showing that IL-1β and TNF-α act as crucial
326 mediators in mammalian IBD models by disrupting epithelial junctions and inducing
327 apoptosis of epithelial cells [53, 54]. Conversely, the key anti-inflammatory cytokines,
328 such as *il10*, were downregulated. These findings highlight an imbalance between pro-
329 inflammatory and anti-inflammatory cytokines in the intestines of Ctla-4-deficient fish.

330 Consistently, the inflammatory signaling pathways associated with these upregulated
331 cytokines, such as the ERK1/2 and MAPK pathways, were positively enriched in
332 inflamed intestines. Single-cell RNA-seq analysis revealed the upregulation and
333 enrichment of these inflammatory cytokines and pathways in neutrophils, macrophages,
334 and B cells of inflamed intestines, indicating their active involvement in inflammatory
335 responses and as major sources of inflammatory signals. Additionally, there was a
336 marked increase in the abundance of Th2 subset cells in the inflamed intestines. These
337 Th2 cells exhibited high expression of *il13* and were significantly enriched in
338 inflammatory signaling pathways, indicating their activated state. Previous research in
339 mammals has identified IL-13 as the key effector Th2 cytokine in ulcerative colitis,
340 directly causing damage to epithelial cells by affecting epithelial tight junctions,
341 apoptosis, and cell restitution [23]. Therefore, upregulated Il13 from Th2 cells may be
342 a significant contributor to epithelial injury in zebrafish model. Notably, the proportion
343 of ILC3-like cells was downregulated in the inflamed intestines, consistent with recent
344 studies reporting a substantial decline of ILC3 in IBD patients [29-31]. ILC3 is the most
345 abundant type of ILCs in the intestines and plays a protective role in IBD in mammals
346 by promoting epithelial cell proliferation and survival, as well as enhancing intestinal
347 barrier function through the production of IL-22 [32, 34]. Thus, the marked decrease in
348 ILC3-like cells may exacerbate intestinal inflammation and damage. Besides, abnormal
349 activation of Th2 cells can lead to dysfunction in downstream B cells and mucosa-
350 associated immunity, which is essential in maintaining the symbiotic bacterial
351 homeostasis in intestines [38]. Thus, a potential correlation may exist between changes

352 in Th2 cells and the observed alterations in the intestinal microbial community in Ctla-
353 4-deficient zebrafish. Overall, our findings provided insights into the occurrence of IBD.
354 However, gaining a comprehensive understanding of the complex interactions among
355 these immune cells, intestinal epithelial cells, and the microbiome in IBD requires
356 further exploration.
357

358 ## Materials and Methods

359 **Experimental fish**

360 Wild-type AB zebrafish (*D rerio*) of both sexes, 4-6 months of age with body
361 weights ranging from 0.3 to 0.8 g and lengths of 3-4 cm, were reared in the laboratory
362 in recirculating water at 26-28 °C under standard conditions as previously described
363 [55]. All animal experiments were performed in accordance with legal regulations and
364 were approved by the Research Ethics Committee of Zhejiang University.

365 **Generation of Ctla-4-deficient zebrafish**

366 CRISPR/Cas9 system was used to knock out the *ctla-4* gene. The targeting
367 sequence 5'-CTCAGAGCCCTACTTCGCAA-3' was designed by optimized CRISPR
368 Design (http://crispr.mit.edu/) and synthesized by T7 RNA polymerase and purified by
369 MEGAclear Kit (AM1908; Invitrogen) *in vitro*. Cas9 protein (500 ng/μl, A45220P;
370 Thermo Fisher Scientific) and purified RNA (90 ng/μl) were coinjected into one cell-
371 stage wild-type embryos. For genotyping, DNA fragment was amplified with primers
372 (F: 5' -TGTGACAGGAAAAGATGGAGAA- 3' and R: 5'-
373 GATCAGATCCACTCCTCCAAAG- 3') and subjected to sequencing. The mutant

374 alleles (-14 bp) were obtained and their offspring were used in experiments.

375 **Histopathological analysis**

376 The anterior, mid, and posterior intestines (n = 3 replicates) were fixed in 4% PFA
377 overnight and embedded in paraffin. The tissues were cut into 4 μm sections and stained
378 with Hematoxylin and eosin (H&E) for pathological analysis. To evaluate the severity
379 of intestinal inflammation, histologic scores were determined according to the criteria
380 supplied by previous publication [22]. Briefly, three independent parameters, including
381 inflammation, extent, and epithelial changes, were assessed and scored as follows: the
382 severity of inflammation (0 = none, 1 = minimal, 2 = mild, 3 = moderate, 4 = marked);
383 the level of inflammation extent (0 = none, 1 = mucosa, 2 = mucosa and submucosa, 3
384 = transmural), the degree of epithelial changes (0 = none, 1 = minimal hyperplasia, 2 =
385 mild hyperplasia, minimal goblet cell loss, 3 = moderate hyperplasia, mild goblet cell
386 loss, 4 = marked hyperplasia with moderate to marked goblet cell loss). Each parameter
387 was calculated and summed to obtain the overall score. The sections were stained with
388 Periodic Acid-Schiff (PAS) reagent to evaluate the number of goblet cells.

389 **RNA-sequencing and bioinformatic analysis**

390 Total RNAs were isolated from wild-type or *ctla-4*$^{-/-}$ intestines (three biological
391 replicates) using TRIzol reagent following the manufacturer's instructions (Takara).
392 cDNA libraries were constructed using NEB Next Ultra Directional RNA Library Prep
393 Kit (NEB), and sequencing was performed according to the Illumina Hiseq2500
394 standard protocol at LC Bio (Hangzhou, China). The differentially expressed genes
395 (DEGs) were identified with absolute Log_2 fold change > 1 and adjusted p-value < 0.05

396 by R package DESeq2. Gene Ontology (GO) enrichment and Kyoto encyclopedia of
397 genes and genomes (KEGG) enrichment analyses were performed by the OmicStudio
398 (http://www.omicstudio.cn/tool) tools. Gene-set enrichment analysis was performed
399 using software GSEA (v4.1.0, https://www.gsea-msigdb.org/gsea/index.jsp), and the
400 heatmap was generated using the R package ggplot2. For the protein-protein interaction
401 (PPI) networks, the DEGs were retrieved in STRING (version 11.5, https://string-
402 db.org/) database (combined score > 0.4), and the PPI network was visualized by
403 Cytoscape software (version 3.9.1) [56]. The betweenness centrality (BC) was
404 calculated using the CytoNCA plugin in Cytoscape software. The RNA-sequencing
405 (RNA-seq) data in this study were deposited in the Gene Expression Omnibus (GEO)
406 (http://www.ncbi.nlm.nih.gov/geo/) database.

407 **Quantitative real-time PCR**

408 Total RNA from intestines was extracted using TRIzol reagent (Takara Bio) and
409 reverse transcribed into cDNAs according to the manufacturer's protocol. PCR
410 experiments were performed in a total volume of 10 μl by using an SYBR Premix Ex
411 Taq kit (Takara Bio). The reaction mixtures were incubated for 2 min at 95°C, then
412 subjected to 40 cycles of 15 s at 95°C, 15 s at 60°C, and 20 s at 72°C. Relative
413 expression levels of the target genes were calculated using the $2^{-\Delta\Delta ct}$ method with β-
414 actin for normalization. Each PCR trial was run in triplicate parallel reactions and
415 repeated three times. The primers used in the experiments are listed in Supplemental
416 Table 1.

417 **Single-cell RNA-sequencing analysis**

418 The intestines from wild-type and *ctla-4*$^{-/-}$ zebrafish were washed by D-Hank's and
419 incubated with D-Hank's containing EDTA (0.37 mg/mL) and DTT (0.14 mg/mL) for
420 20 min. The resulting supernatants were collected as fraction 1. The remaining tissues
421 were subsequently digested with type IV collagenase (0.15 mg/mL) for 1 h at room
422 temperature and the resulting supernatants were collected as fraction 2. Fractions 1 and
423 2 were combined and centrifuged at 350 g for 10 min. Cells were then washed with D-
424 Hank's and suspended in 40% percoll (percoll : FBS: L-15 medium = 4 : 1: 5) and
425 passed through a 40-μm strainer. The cell suspension was carefully layered onto 63%
426 percoll (percoll : FBS : L-15 medium = 6.3 : 1: 2.7) and centrifuged at 400 g for 30 min
427 at room temperature. The cell layer of the interface was collected and washed with D-
428 Hank's at 400 g for 10 min. Cell quantity and viability were assessed using 0.4% trypan
429 blue staining, revealing that over 90% of the cells were viable. Single-cell samples were
430 submitted to the LC-Bio Technology Co., Ltd (Hangzhou, China) for 10× Genomics
431 library preparation and data analysis assistance. Libraries were prepared using the
432 Chromium™ Controller and Chromium™ Single Cell 3' Library & Gel Bead Kit v2
433 (10× Genomics) according to the manufacturer's protocol, and sequenced on an
434 Illumina NovaSeq 6000 sequencing system (paired-end multiplexing run, 150 bp) at a
435 minimum depth of 20,000 reads per cell. Sequencing results were demultiplexed and
436 converted to FASTQ format using Illumina bcl2fastq software and the data were
437 aligned to Ensembl zebrafish genome assembly GRCz11. Quality control was
438 performed using the Seurat. DoubletFinder R package was used to identify and filter
439 the doublets (multiplets) [57]. The cells were removed if they expressed fewer than 500

unique genes, or > 60% mitochondrial reads. The number of cells after filtration in the current study was 3,263 in wild-type and 4,276 in *ctla-4*$^{-/-}$ groups, respectively. Cells were grouped into an optimal number of clusters for *de novo* cell type discovery using Seurat's FindNeighbors() and FindClusters() functions, graph-based clustering approach with visualization of cells being achieved through the use of t-SNE or UMAP plots [58]. The cell types were determined using a combination of marker genes identified from the literature and gene ontology. The marker genes were visualized by dot plot and t-SNE plots to reveal specific individual cell types.

In vivo administration of sCtla-4-Ig

An *in vivo* sCtla-4-Ig administration assay was conducted to evaluate the potential therapeutic effect of sCTLA-4-Ig on intervention of a *ctla-4*-deficiency induced IBD-like phenotype. For this procedure, the *ctla-4*$^{-/-}$ zebrafish were i.p administered with recombinant soluble Ctla-4-Ig protein (sCtla-4-Ig, 2 μg/g body weight) every other day until day 14. Fish that received an equal amount of human IgG isotype were used as control. The dose of sCtla-4-Ig was chosen based on its ability to significantly inhibit the mRNA expression of *il13* in Ctla-4-deficient zebrafish.

Statistical analysis

Statistical analysis and graphical presentation were performed with GraphPad Prism 8.0. All data were presented as the mean ± SD of each group. Statistical evaluation of differences was assessed using one-way ANOVA, followed by an unpaired two-tailed *t*-teat. Statistical significance was defined as $^{*}p < 0.05$, $^{**}p < 0.01$, $^{***}p < 0.001$, and $^{****}p < 0.0001$. All experiments were replicated at least three times.

Data availability

All data generated or analyzed during this study are included in this article and its supplementary information files. The RNA-seq and scRNA-seq data for this study have been deposited in NCBI Gene Expression Omnibus (GEO) (https://www.ncbi.nlm.nih.gov/geo/) under accession numbers GSE255304 and GSE255303, respectively. The 16S rRNA sequencing data in this study have been deposited in the NCBI Sequence Read Archive (SRA) (https://www.ncbi.nlm.nih.gov/sra/) with an accession number of BioProject PRJNA1073727.

Acknowledgements

We are grateful to Bio-ultrastructure analysis Lab of Analysis center of Agrobiology and environmental sciences, Zhejiang Univ in the TEM sample preparation and observation. We thank Hong Deng and Qiong Huang for advice and expertise in pathological analysis. We also thank She-long Zhang for two-photon laser confocal scanning microscope capture. This work was supported by grants from the National Natural Science Foundation of China (32173003), the National Key Research and Development Program of China (2018YFD0900503, 2018YFD0900505).

Author Contributions

L. L. Q. and J. Z. S. conceived and designed the experiments. L. L. Q. and C. B.

484 H. performed the experiments. L. L. Q., C. B. H., Q. Z., Y. W., A. F. L., L. X. X., Y.
485 C., and J. Z. S. analyzed the data. L. X. X., D. D. F., and J. Z. S. contributed
486 reagents/materials/analysis tools. L. L. Q., Y. C., L. X. X. and J. Z. S. wrote the
487 manuscript. All authors reviewed the paper and provided comments.

488

489 **Conflict of Interest**

490 The authors declare that they have no competing financial interests.

491

492 **Ethical approval and consent to participate**

493 All animal experiments were performed with the approval of the Ethics Committee for
494 Animal Experimentation of Zhejiang University.

495

496 **REFERENCES**

497 1. Hodson R (2016) Inflammatory bowel disease. Nature 540:S97-S97.
498 https://10.1038/540S97a
499 2. Zhang Y Z, Li Y Y (2014) Inflammatory bowel disease: Pathogenesis. World J Gastroentero
500 20:91-99. https://10.3748/wjg.v20.i1.91
501 3. Venema W T C U, Voskuil M D, Dijkstra G, Weersma R K, Festen E A M (2017) The genetic
502 background of inflammatory bowel disease: from correlation to causality. J Pathol
503 241:146-158. https://10.1002/path.4817
504 4. Loftus E V (2004) Clinical epidemiology of inflammatory bowel disease: Incidence,
505 prevalence, and environmental influences. Gastroenterology 126:1504-1517.
506 https://10.1053/j.gastro.2004.01.063
507 5. Khor B, Gardet A, Xavier R J (2011) Genetics and pathogenesis of inflammatory bowel
508 disease. Nature 474:307-317. https://10.1038/nature10209
509 6. Neurath M F (2020) Host-microbiota interactions in inflammatory bowel disease. Nat Rev
510 Gastro Hepat 17:76-77. https://10.1038/s41575-019-0248-1
511 7. Kordjazy N, Haj-Mirzaian A, Haj-Mirzaian A, Rohani M M, Gelfand E W, Rezaei N *et al.*
512 (2018) Role of toll-like receptors in inflammatory bowel disease. Pharmacological
513 Research 129:204-215. https://10.1016/j.phrs.2017.11.017
514 8. Horowitz J E, Warner N, Staples J, Crowley E, Gosalia N, Murchie R *et al.* (2021) Mutation

515 spectrum of NOD2 reveals recessive inheritance as a main driver of Early Onset Crohn's
516 Disease. Sci Rep-Uk 11:5595. https://10.1038/s41598-021-84938-8
517 9. Duerr R H, Taylor K D, Brant S R, Rioux J D, Silverberg M S, Daly M J *et al.* (2006) A genome-
518 wide association study identifies IL23R as an inflammatory bowel disease gene. Science
519 314:1461-1463. https://10.1126/science.1135245
520 10. Tremelling M, Berzuini C, Massey D, Bredin F, Price C, Dawson C *et al.* (2008) Contribution
521 of TNFSF15 gene variants to Crohn's disease susceptibility confirmed in UK population.
522 Inflamm Bowel Dis 14:733-737. https://10.1002/ibd.20399
523 11. Marengere L E, Waterhouse P, Duncan G S, Mittrucker H W, Feng G S, Mak T W (1996)
524 Regulation of T cell receptor signaling by tyrosine phosphatase SYP association with
525 CTLA-4. Science 272:1170-1173. https://10.1126/science.272.5265.1170
526 12. Lee K M, Chuang E, Griffin M, Khattri R, Hong D K, Zhang W G *et al.* (1998) Molecular basis
527 of T cell inactivation by CTLA-4. Science 282:2263-2266.
528 https://10.1126/science.282.5397.2263
529 13. Yokosuka T, Kobayashi W, Takamatsu M, Sakata-Sogawa K, Zeng H, Hashimoto-Tane A
530 *et al.* (2010) Spatiotemporal Basis of CTLA-4 Costimulatory Molecule-Mediated Negative
531 Regulation of T Cell Activation. Immunity 33:326-339.
532 https://10.1016/j.immuni.2010.09.006
533 14. Linsley P S, Greene J L, Brady W, Bajorath J, Ledbetter J A, Peach R (1994) Human B7-1
534 (Cd80) and B7-2 (Cd86) Bind with Similar Avidities but Distinct Kinetics to Cd28 and Ctla-
535 4 Receptors. Immunity 1:793-801. https://10.1016/S1074-7613(94)80021-9
536 15. Collins A V, Brodie D W, Gilbert R J, Iaboni A, Manso-Sancho R, Walse B *et al.* (2002) The
537 interaction properties of costimulatory molecules revisited. Immunity 17:201-210.
538 https://10.1016/s1074-7613(02)00362-x
539 16. Saito T, Yokosuka T, Hashimoto-Tane A (2010) Dynamic regulation of T cell activation and
540 co-stimulation through TCR-microclusters. Febs Lett 584:4865-4871.
541 https://10.1016/j.febslet.2010.11.036
542 17. Repnik K, Potocnik U (2010) CT60 Single-Nucleotide Polymorphism Is Associated with
543 Slovenian Inflammatory Bowel Disease Patients and Regulates Expression of Isoforms.
544 DNA Cell Biol 29:603-610. https://10.1089/dna.2010.1021
545 18. Xia B, Crusius J B A, Wu J, Zwiers A, van Bodegraven A A, Peña A S (2002) CTLA-4 gene
546 polymorphisms in Dutch and Chinese patients with inflammatory bowel disease. Scand J
547 Gastroentero 37:1296-1300. https://10.1080/003655202761020579
548 19. Jiang T, Ge L Q, Chen Z T, Li C, Zhou F, Luo Y *et al.* (2010) Effect of cytotoxic T lymphocyte-
549 associated molecule 4 1661 gene polymorphism on its expression and transcription in
550 ulcerative colitis. J Digest Dis 11:369-375. https://10.1111/j.1751-2980.2010.00462.x
551 20. Bamias G, Delladetsima I, Perdiki M, Siakavellas S I, Goukos D, Papatheodoridis G V *et al.*
552 (2017) Immunological Characteristics of Colitis Associated with Anti-CTLA-4 Antibody
553 Therapy. Cancer Invest 35:443-455. https://10.1080/07357907.2017.1324032
554 21. Lo B C, Kryczek I, Yu J, Vatan L, Caruso R, Matsumoto M *et al.* (2024) Microbiota-
555 dependent activation of CD4+ T cells induces CTLA-4 blockade–associated colitis via Fcγ
556 receptors. Science 383:62-70. https://10.1126/science.adh8342
557 22. Erben U, Loddenkemper C, Doerfel K, Spieckermann S, Haller D, Heimesaat M M *et al.*
558 (2014) A guide to histomorphological evaluation of intestinal inflammation in mouse

559 models. Int J Clin Exp Pathol 7:4557-4576.
560 23. Heller F, Florian P, Bojarski C, Richter J, Christ M, Hillenbrand B *et al.* (2005) Interleukin-13
561 is the key effector Th2 cytokine in ulcerative colitis that affects epithelial tight junctions,
562 apoptosis, and cell restitution. Gastroenterology 129:550-564.
563 https://10.1016/j.gastro.2005.05.002
564 24. Butin-Israeli V, Bui T M, Wiesolek H L, Mascarenhas L, Lee J J, Mehl L C *et al.* (2019)
565 Neutrophil-induced genomic instability impedes resolution of inflammation and wound
566 healing. J Clin Invest 129:712-726. https://10.1172/JCI122085
567 25. Lees C W, Barrett J C, Parkes M, Satsangi J (2011) New IBD genetics: common pathways
568 with other diseases. Gut 60:1739-1753. https://10.1136/gut.2009.199679
569 26. Lee J C, Biasci D, Roberts R, Gearry R B, Mansfield J C, Ahmad T *et al.* (2017) Genome-
570 wide association study identifies distinct genetic contributions to prognosis and
571 susceptibility in Crohn's disease. Nat Genet 49:262-268. https://10.1038/ng.3755
572 27. Sinkala M, Nkhoma P, Mulder N, Martin D P (2021) Integrated molecular characterisation
573 of the MAPK pathways in human cancers reveals pharmacologically vulnerable mutations
574 and gene dependencies. Communications Biology 4:https://10.1038/s42003-020-01552-
575 6
576 28. Trebak M, Kinet J P (2019) Calcium signalling in T cells. Nature Reviews Immunology
577 19:154-169. https://10.1038/s41577-018-0110-7
578 29. Bernink J H, Peters C P, Munneke M, te Velde A A, Meijer S L, Weijer K *et al.* (2013) Human
579 type 1 innate lymphoid cells accumulate in inflamed mucosal tissues. Nat Immunol
580 14:221-229. https://10.1038/ni.2534
581 30. Li J, Doty A L, Tang Y, Berrie D, Iqbal A, Tan S A *et al.* (2017) Enrichment of IL-17A(+) IFN-
582 gamma(+) and IL-22(+) IFN-gamma(+) T cell subsets is associated with reduction of
583 NKp44(+) ILC3s in the terminal ileum of Crohn's disease patients. Clin Exp Immunol
584 190:143-153. https://10.1111/cei.12996
585 31. Martin J C, Chang C, Boschetti G, Ungaro R, Giri M, Grout J A *et al.* (2019) Single-Cell
586 Analysis of Crohn's Disease Lesions Identifies a Pathogenic Cellular Module Associated
587 with Resistance to Anti-TNF Therapy. Cell 178:1493-1508 e1420.
588 https://10.1016/j.cell.2019.08.008
589 32. Buonocore S, Ahern P P, Uhlig H H, Ivanov, II, Littman D R, Maloy K J *et al.* (2010) Innate
590 lymphoid cells drive interleukin-23-dependent innate intestinal pathology. Nature
591 464:1371-1375. https://10.1038/nature08949
592 33. Ermann J, Staton T, Glickman J N, de Waal Malefyt R, Glimcher L H (2014) Nod/Ripk2
593 signaling in dendritic cells activates IL-17A-secreting innate lymphoid cells and drives
594 colitis in T-bet-/-.Rag2-/- (TRUC) mice. Proc Natl Acad Sci U S A 111:E2559-2566.
595 https://10.1073/pnas.1408540111
596 34. Aparicio-Domingo P, Romera-Hernandez M, Karrich J J, Cornelissen F, Papazian N,
597 Lindenbergh-Kortleve D J *et al.* (2015) Type 3 innate lymphoid cells maintain intestinal
598 epithelial stem cells after tissue damage. J Exp Med 212:1783-1791.
599 https://10.1084/jem.20150318
600 35. Ott S J, Musfeldt M, Wenderoth D F, Hampe J, Brant O, Folsch U R *et al.* (2004) Reduction
601 in diversity of the colonic mucosa associated bacterial microflora in patients with active
602 inflammatory bowel disease. Gut 53:685-693. https://10.1136/gut.2003.025403

36. Manichanh C, Rigottier-Gois L, Bonnaud E, Gloux K, Pelletier E, Frangeul L *et al.* (2006) Reduced diversity of faecal microbiota in Crohn's disease revealed by a metagenomic approach. Gut 55:205-211. https://10.1136/gut.2005.073817
37. Zhao Q, Chang H, Zheng J, Li P, Ye L, Pan R *et al.* (2023) A novel Trmt5-deficient zebrafish model with spontaneous inflammatory bowel disease-like phenotype. Signal Transduct Target Ther 8:86. https://10.1038/s41392-023-01318-6
38. Xu Z, Takizawa F, Casadei E, Shibasaki Y, Ding Y, Sauters T J C *et al.* (2020) Specialization of mucosal immunoglobulins in pathogen control and microbiota homeostasis occurred early in vertebrate evolution. Sci Immunol 5:https://10.1126/sciimmunol.aay3254
39. Belzer C, de Vos W M (2012) Microbes inside--from diversity to function: the case of Akkermansia. ISME J 6:1449-1458. https://10.1038/ismej.2012.6
40. Waterhouse P, Penninger J M, Timms E, Wakeham A, Shahinian A, Lee K P *et al.* (1995) Lymphoproliferative Disorders with Early Lethality in Mice Deficient in Ctla-4. Science 270:985-988. https://10.1126/science.270.5238.985
41. Tivol E A, Borriello F, Schweitzer A N, Lynch W P, Bluestone J A, Sharpe A H (1995) Loss of Ctla-4 Leads to Massive Lymphoproliferation and Fatal Multiorgan Tissue Destruction, Revealing a Critical Negative Regulatory Role of Ctla-4. Immunity 3:541-547. https://10.1016/1074-7613(95)90125-6
42. Hosseini A, Gharibi T, Marofi F, Babaloo Z, Baradaran B (2020) CTLA-4: From mechanism to autoimmune therapy. Int Immunopharmacol 80:106221. https://10.1016/j.intimp.2020.106221
43. Sun W H, Zhang X M, Wu J, Zhao W D, Zhao S X, Li M L (2019) Correlation of TSHR and CTLA-4 Single Nucleotide Polymorphisms with Graves Disease. Int J Genomics 2019:6982623. https://10.1155/2019/6982623
44. Vergara A, De Felice M, Cesaro A, Gragnano F, Pariggiano I, Golia E *et al.* (2023) Immune-Checkpoint Inhibitor-Related Myocarditis: Where We Are and Where We Will Go. Angiology 12:33197231201929. https://10.1177/00033197231201929
45. Kheiralla K E K (2021) CTLA-4 (+49A/G) Polymorphism in Type 1 Diabetes Children of Sudanese Population. Glob Med Genet 8:11-18. https://10.1055/s-0041-1723008
46. Lin T W, Hu Y C, Yang Y H, Chien Y H, Lee N C, Yu H H *et al.* (2022) CTLA-4 gene mutation and multiple sclerosis: A case report and literature review. J Microbiol Immunol 55:545-548. https://10.1016/j.jmii.2021.10.009
47. Cutolo M, Sulli A, Paolino S, Pizzorni C (2016) CTLA-4 blockade in the treatment of rheumatoid arthritis: an update. Expert Rev Clin Immu 12:417-425. https://10.1586/1744666x.2016.1133295
48. Chang M C, Chang Y T, Tien Y W, Liang P C, Jan I S, Wei S C *et al.* (2007) T-Cell regulatory gene CTLA-4 Polymorphism/Haplotype association with autoimmune pancreatitis. Clin Chem 53:1700-1705. https://10.1373/clinchem.2007.085951
49. Fathima N, Narne P, Ishaq M (2019) Association and gene-gene interaction analyses for polymorphic variants in CTLA-4 and FOXP3 genes: role in susceptibility to autoimmune thyroid disease. Endocrine 64:591-604. https://10.1007/s12020-019-01859-3
50. Zeissig S, Petersen B S, Tomczak M, Melum E, Huc-Claustre E, Dougan S K *et al.* (2015) Early-onset Crohn's disease and autoimmunity associated with a variant in CTLA-4. Gut 64:1889-1897. https://10.1136/gutjnl-2014-308541

51. Angelino G, Cifaldi C, Zangari P, Di Cesare S, Di Matteo G, Chiriaco M *et al.* (2021) Gastric cancer, inflammatory bowel disease and polyautoimmunity in a 17-year-old boy: CTLA-4 deficiency successfully treated with Abatacept. Eur J Gastroen Hepat 33:E1051-E1056. https://10.1097/Meg.0000000000002185
52. Liu J Z, van Sommeren S, Huang H L, Ng S C, Alberts R, Takahashi A *et al.* (2015) Association analyses identify 38 susceptibility loci for inflammatory bowel disease and highlight shared genetic risk across populations. Nat Genet 47:979-+. https://10.1038/ng.3359
53. Al-Sadi R, Guo S H, Ye D M, Dokladny K, Alhmoud T, Ereifej L *et al.* (2013) Mechanism of IL-1b Modulation of Intestinal Epithelial Barrier Involves p38 Kinase and Activating Transcription Factor-2 Activation. Journal of Immunology 190:6596-6606. https://10.4049/jimmunol.1201876
54. Al-Sadi R, Guo S H, Ye D M, Ma T Y (2013) TNF-α Modulation of Intestinal Epithelial Tight Junction Barrier Is Regulated by ERK1/2 Activation of Elk-1. Am J Pathol 183:1871-1884. https://10.1016/j.ajpath.2013.09.001
55. Zhu L Y, Lin A F, Shao T, Nie L, Dong W R, Xiang L X *et al.* (2014) B Cells in Teleost Fish Act as Pivotal Initiating APCs in Priming Adaptive Immunity: An Evolutionary Perspective on the Origin of the B-1 Cell Subset and B7 Molecules. Journal of Immunology 192:2699-2714. https://10.4049/jimmunol.1301312
56. Kohl M, Wiese S, Warscheid B (2011) Cytoscape: software for visualization and analysis of biological networks. Methods Mol Biol 696:291-303. https://10.1007/978-1-60761-987-1_18
57. McGinnis C S, Murrow L M, Gartner Z J (2019) DoubletFinder: Doublet Detection in Single-Cell RNA Sequencing Data Using Artificial Nearest Neighbors. Cell Syst 8:329-+. https://10.1016/j.cels.2019.03.003
58. Cronan M R, Hughes E J, Brewer W J, Viswanathan G, Hunt E G, Singh B *et al.* (2021) A non-canonical type 2 immune response coordinates tuberculous granuloma formation and epithelialization. Cell 184:1757-1774 e1714. https://10.1016/j.cell.2021.02.046
59. Hu C B, Wang J, Hong Y, Li H, Fan D D, Lin A F *et al.* (2023) Single-cell transcriptome profiling reveals diverse immune cell populations and their responses to viral infection in the spleen of zebrafish. Faseb J 37:e22951. https://10.1096/fj.202201505RRRR

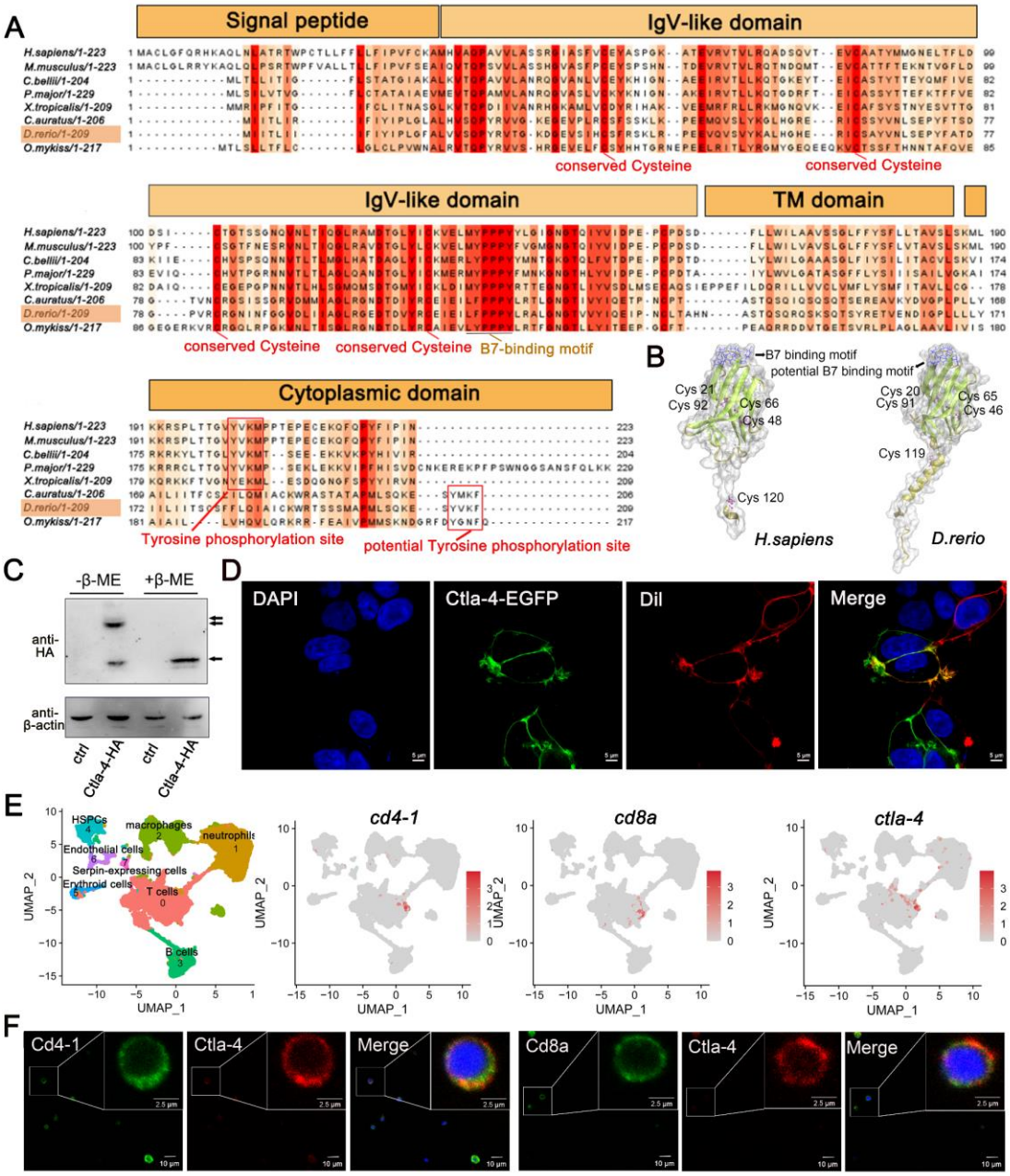

Fig.1 Characterization of zebrafish Ctla-4. **A** Alignment of the Ctla-4 homologues from different species generated with ClustalX and Jalview. The conserved and partially conserved amino acid residues in each species are colored in hues graded from orange to red, respectively. The conserved Cysteine residues, and conserved functional motifs, such as B7-binding motif, Tyrosine phosphorylation site, and potential Tyrosine phosphorylation site were indicated separately. The signal peptide, IgV-like domain, transmembrane (TM) domain and cytoplasmic domain were marked at the top of the

688 sequence. **B** Tertiary protein structures of Ctla-4 ectodomains between humans and
689 zebrafish were predicted by AlphaFold2. The two pairs of disulfide bonds (Cys^{20}-
690 Cys^{91}/Cys^{46}-Cys^{65} in zebrafish and Cys^{21}-Cys^{92}/Cys^{48}-Cys^{66} in humans) used to connect
691 the two-layer β-sandwich, and the separate Cys residue (Cys^{119} in zebrafish and Cys^{120}
692 in humans) associated with the dimerization of the proteins are indicated. The Cys
693 residues are represented in purple ball-and-stick and the identified or potential B7
694 binding sites are highlighted in blue. **C** Dimer of Ctla-4 was identified by Western blot
695 under reducing (+β-ME) or non-reducing (-β-ME) conditions. The ctrl represents the
696 empty control plasmid. The monomer is indicated by one arrow, the dimer by two
697 arrows. **D** The subcellular localization of Ctla-4 protein was assessed in HEK293T cells
698 transfected with pEGFPN1-Ctla-4 for 48 hours using a two-photon laser-scanning
699 microscope (Original magnification, 630×). The nucleus was stained with DAPI (blue),
700 the cell membrane was stained with DiI (red). **E** tSNE plots show the relative
701 distribution of common T cell markers *cd4-1*, *cd8a* and *ctla-4*. The data are from splenic
702 single cell RNA sequencing (scRNA-seq) dataset we recently established [59]. **F**
703 Immunofluorescence staining of lymphocytes separated from blood, spleens, and
704 kidneys of zebrafish. Cells were stained with mouse anti-Ctla-4, together with rabbit
705 anti-Cd4-1 or rabbit anti-Cd8α. DAPI stain shows the location of the nuclei. The images
706 were obtained by two-photon laser-scanning microscope (Original magnification,
707 630×).

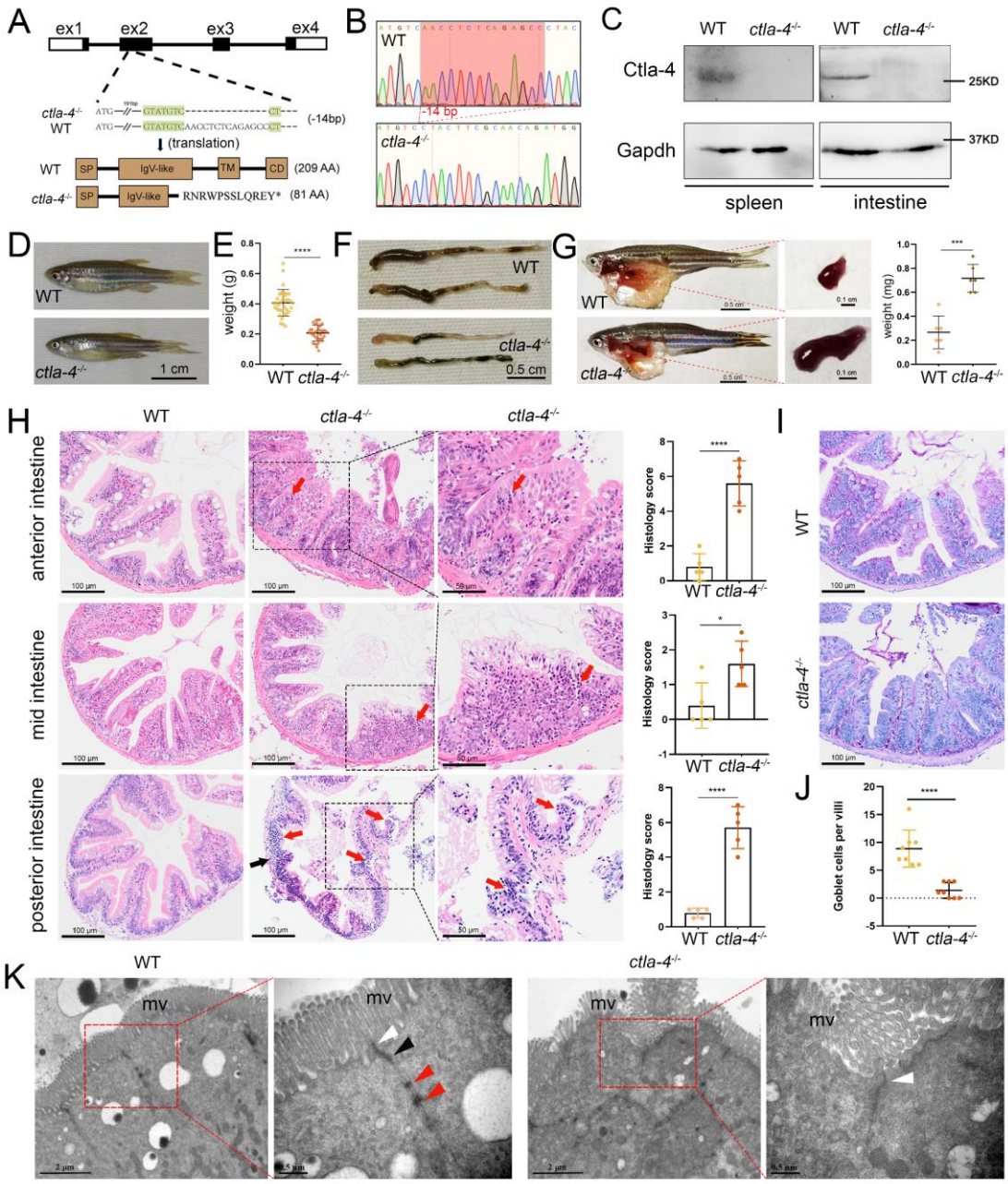

Fig.2 Examination on the IBD-like phenotype in *ctla-4*$^{-/-}$ zebrafish. **A** Generation of a homozygous *ctla-4*-deficient (*ctla-4*$^{-/-}$) zebrafish line through CRISPR/Cas9-based knockout of *ctla-4* gene on chromosome 9. A 14-bp deletion mutation in exon 2 results in a premature stop at codon 82, which is predicted to produce a defective Ctla-4 protein containing 81 amino acids. **B** Genotyping of the deficiency of *ctla-4* gene by Sanger sequencing. **C** Knockout efficiency of Ctla-4 selectively examined in spleen and gut

715 tissues of *ctla-4*$^{-/-}$ zebrafish by Western blot analysis. Gapdh serves as a loading control.
716 **D** Normal gross appearance of adult wild-type (WT) and *ctla-4*$^{-/-}$ zebrafish. **E** Body
717 weight statistics of WT and *ctla-4*$^{-/-}$ zebrafish (n = 30). **F** The change of intestine length
718 in WT and *ctla-4*$^{-/-}$ zebrafish. **G** The change of splenic size in WT and *ctla-4*$^{-/-}$ zebrafish.
719 **H** Representative H＆E staining analysis of histopathological changes and quantitation
720 of histology score in anterior, mid and posterior intestines from WT and *ctla-4*$^{-/-}$
721 zebrafish. Red arrows indicate mucosal inflammatory cell infiltration, and black arrow
722 indicates transmural inflammatory cell infiltration. **I** PAS analysis indicates goblet cells
723 in anterior intestine from WT and *ctla-4*$^{-/-}$ zebrafish. **J** Quantitation analysis of goblet
724 cells of each villus in the foregut of WT and *ctla-4*$^{-/-}$ zebrafish (n = 8). **K** Observation
725 of cell junctions between intestinal epithelial cells in posterior intestines from WT and
726 *ctla-4*$^{-/-}$ zebrafish under TEM (Hitachi Model H-7650). White triangles indicate tight
727 junctions, black triangle indicates adhesion junctions, and red triangles indicate
728 desmosomes. Data are presented as mean ± standard deviation (SD). Statistical
729 significance was assessed through an unpaired Student's t test ($^{*}p < 0.05$; $^{**}p < 0.01$;
730 $^{***}p < 0.001$; $^{****}p < 0.0001$).

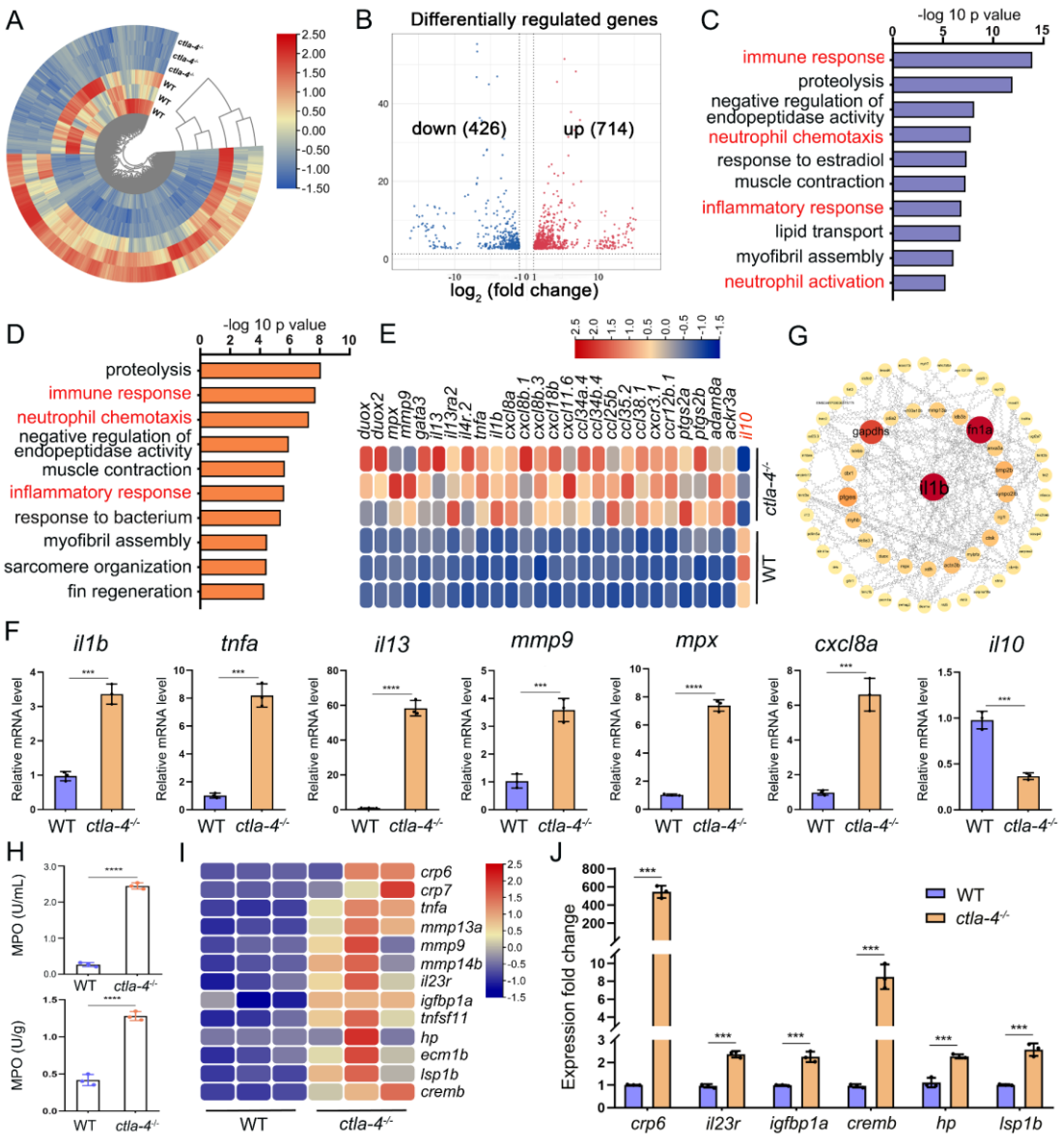

731

732 **Fig.3** RNA-sequencing analysis of the molecular implications associated with the IBD-

733 like phenotype in *ctla-4*$^{-/-}$ zebrafish. **A** Heatmap of different expressed genes between

734 the intestines from wild-type (WT) and *ctla-4*$^{-/-}$ zebrafish. **B** Volcano plot showing the

735 up-/down-regulated genes in the intestines of *ctla-4*$^{-/-}$ zebrafish compared with those of

736 WT zebrafish. Red indicates up-regulated genes and blue indicates down-regulated

737 genes. **C** GO analysis showing top 10 terms in biological processes of DEGs. **D** GO

738 analysis showing top 10 terms in biological processes of all up-regulated genes. **E**

739 Heatmap of representative differently expressed inflammation and chemotaxis-related

genes. **F** The mRNA expression levels of important genes associated with inflammation and chemokines confirmed by real-time qPCR. **G** Protein-protein interaction network was constructed using the DEGs. The nodes represent the proteins (genes); the edges represent the interaction of proteins (genes). **H** The MPO activity in the intestines (up) and peripheral blood (down). **I** Heatmap of IBD biomarker genes and IBD-related genes. **J** The mRNA expression levels of representative IBD biomarker genes and IBD-related genes were analyzed by real-time qPCR. Data are presented as mean ± standard deviation (SD). Statistical significance was assessed through an unpaired Student's t test ($^{**}p < 0.01$; $^{***}p < 0.001$; $^{****}p < 0.0001$).

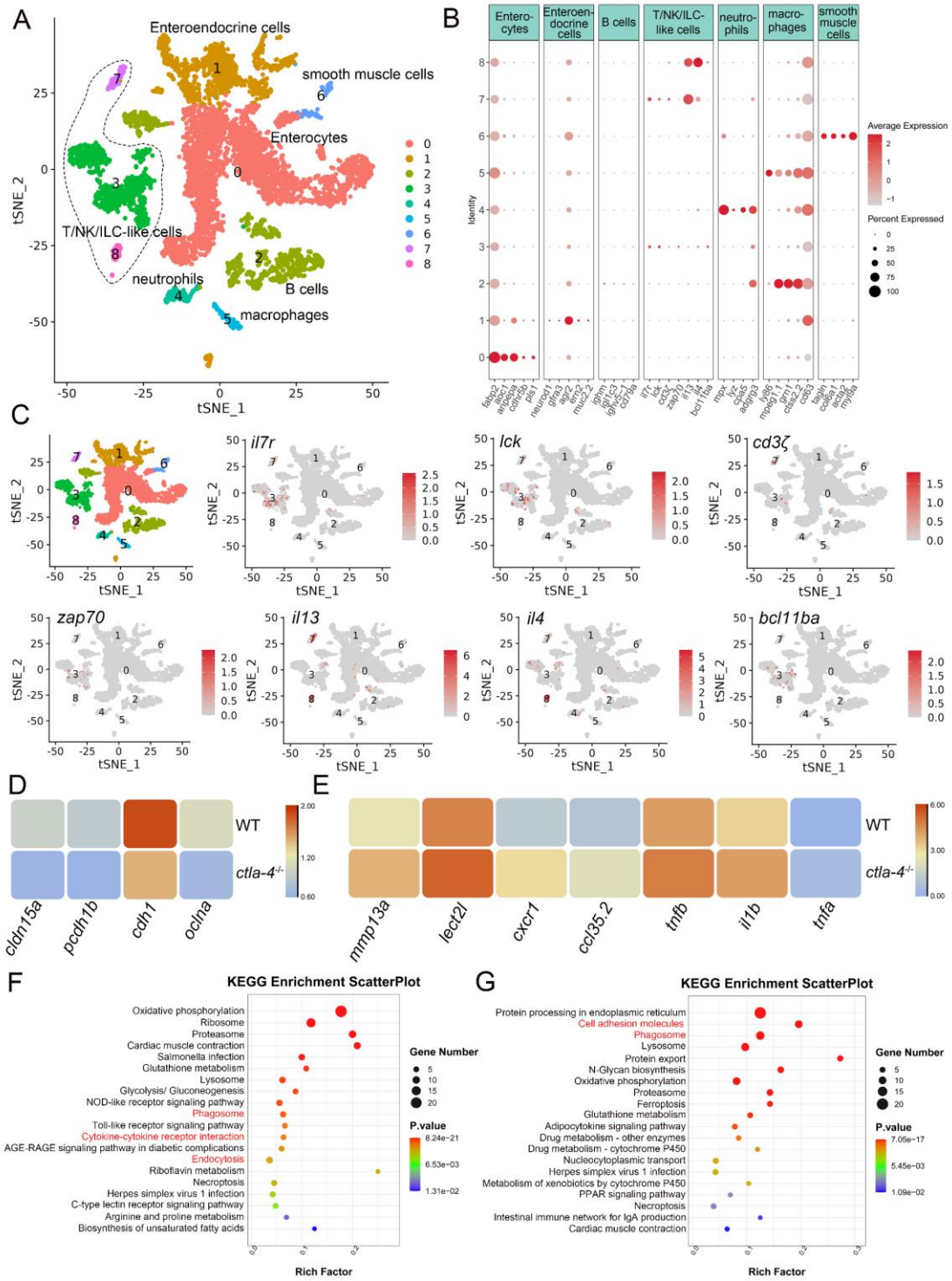

Fig.4 Single cell RNA-sequencing analysis of the major cell types associated with the IBD-like phenotype in *ctla-4*$^{-/-}$ zebrafish. **A** Classification of cell types from zebrafish intestines by tSNE nonlinear clustering. **B** Dot plot showing the expression levels of lineage marker genes and percentage of cells per cluster that express the gene of interest.

754 **C** Expression maps of T cell associated markers within the cell populations of the
755 zebrafish intestines. **D** Heatmap of the tight/adhesion junction-related genes in
756 enterocytes among the samples from wild-type (WT) and *ctla-4*$^{-/-}$ zebrafish. **E** Heatmap
757 of inflammation-related genes involved in cytokine-cytokine receptor interaction in
758 neutrophils among the samples from WT and *ctla-4*$^{-/-}$ zebrafish. **F** KEGG enrichment
759 analysis showing the top 15 terms of up-regulated genes in neutrophils from the *ctla-4*$^{-}$
760 $^{/-}$ sample versus the WT sample. **G** KEGG enrichment analysis showing the top 15
761 terms of up-regulated genes in macrophages from the *ctla-4*$^{-/-}$ sample versus the WT
762 sample.

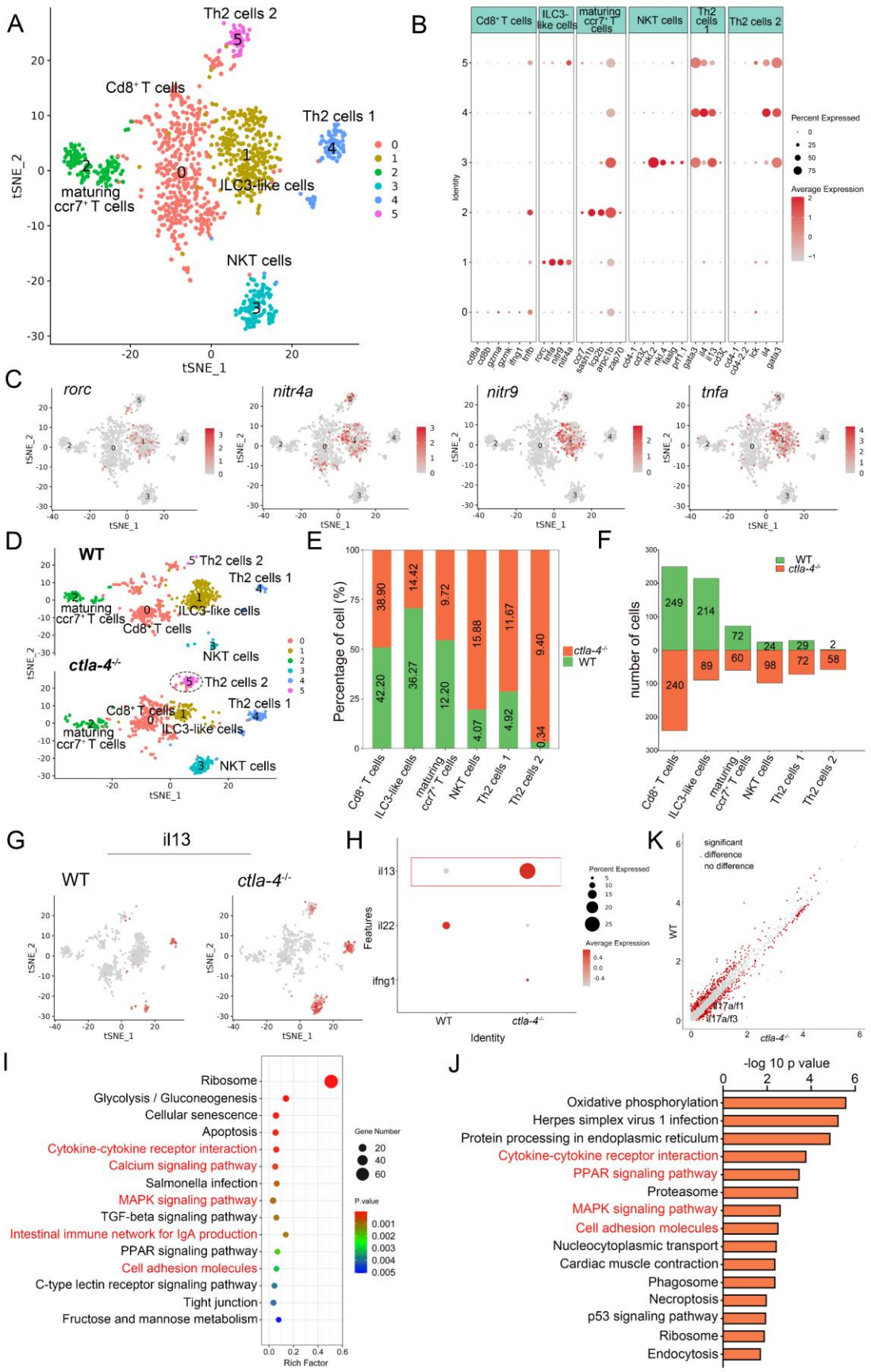

Fig.5 Single cell RNA-sequencing analysis of the subset immune-cells associated with

765 the IBD-like phenotype in *ctla-4*$^{-/-}$ zebrafish. **A** Classification of subset cells from the
766 T/NK/ILC-like group by tSNE nonlinear clustering. **B** Dot plot showing the expression
767 levels of subset marker genes and percentage of cells per cluster that express the gene
768 of interest. **C** Marker gene expression in individual cluster identifying this cluster as
769 ILC3-like cells. **D** Changes in the composition of subset cells between samples from
770 wild-type (WT) and *ctla-4*$^{-/-}$ zebrafish. A significantly increased Th2 subset (referred to
771 as Th2 cells 2) in the *ctla-4*$^{-/-}$ sample was highlighted with a black dashed circle. **E**
772 Histogram showing the different ratios of subset cells between the WT and *ctla-4*$^{-/-}$
773 samples. **F** Histogram presenting the different numbers of subset cells between the WT
774 and *ctla-4*$^{-/-}$ samples. **G** Expression maps of the cytokine *il13* within different subset
775 cells between the WT and *ctla-4*$^{-/-}$ samples. **H** Dot plots illustrating the differential
776 expression of *il13* in T/NK/ILC-like cells from WT and *ctla-4*$^{-/-}$ zebrafish. **I** KEGG
777 enrichment analysis showing the top 15 terms of up-regulated genes in the subset of
778 Th2 cells 2. **J** KEGG enrichment analysis showing the top 15 terms of up-regulated
779 genes in NKT cells. **K** Scatter plot showing the DEGs of ILC3-like cells in WT and
780 *ctla-4*$^{-/-}$ zebrafish. The *il17a/f1* and *il17a/f3* was shown in the scatter plot.

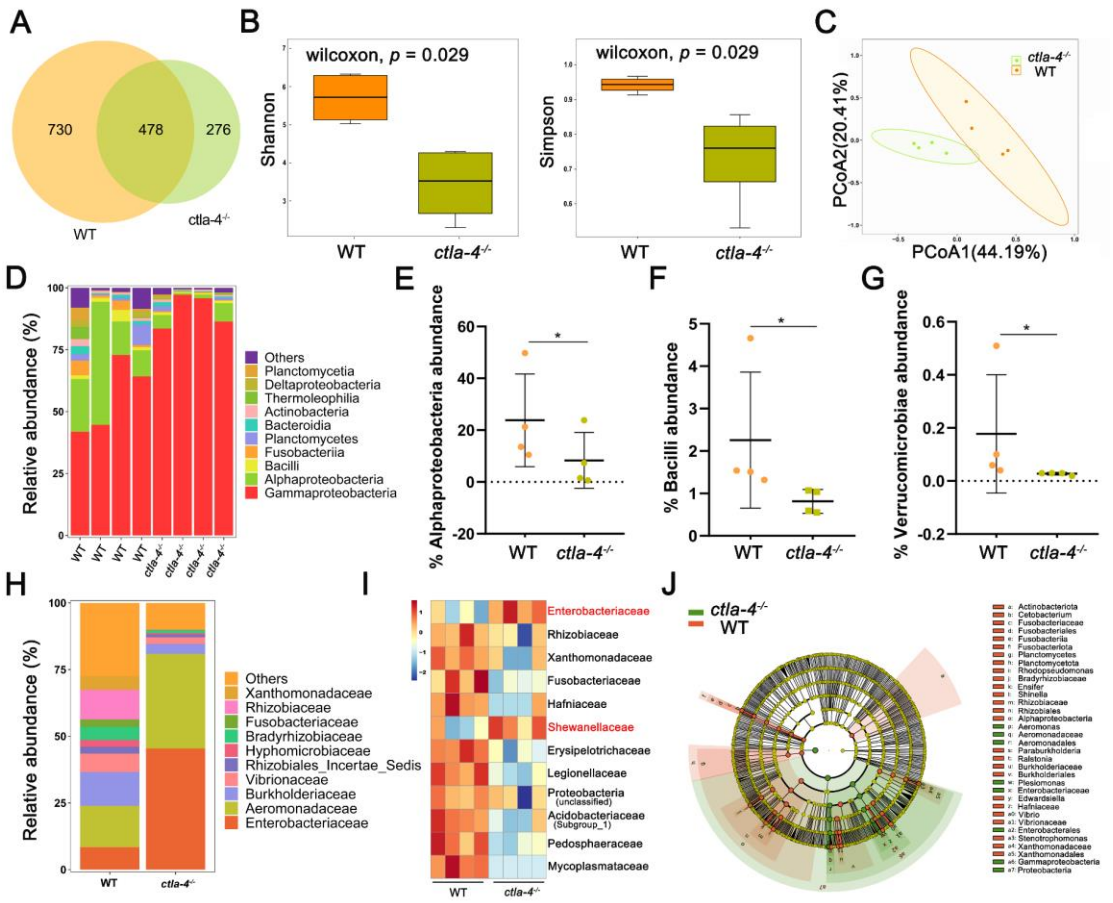

Fig.6 Alteration in microbial composition in the intestines of *ctla-4*$^{-/-}$ zebrafish. **A** Venn diagram showing the number of ASVs in zebrafish intestinal microbiota. **B** Alpha-diversity of microbes was calculated through Shannon index and Simpson index. **C** Beta-diversity analyzed based on PCoA was shown by using Bray Curtis distance. **D** The relative abundance of intestinal microbiota at the class level. **E-G** The relative abundance of Alphaproteobacteria (**E**), Bacilli (**F**) and verrucomicrobiae (**G**) in the intestines from the wild-type (WT) and *ctla-4*$^{-/-}$ zebrafish. $^{*}p < 0.05$. **H** The relative abundance of intestinal microbiota at the family level. **I** Heatmap analysis of the differential abundances of bacterial communities at family level in the WT and *ctla-4*$^{-/-}$ zebrafish ($p < 0.05$). **J** Cladogram representation of LEfSe analysis showing the differentially abundant bacterial taxa between the intestines from WT (red) and *ctla-4*$^{-}$

$^{/-}$ (green) zebrafish ($p < 0.05$).

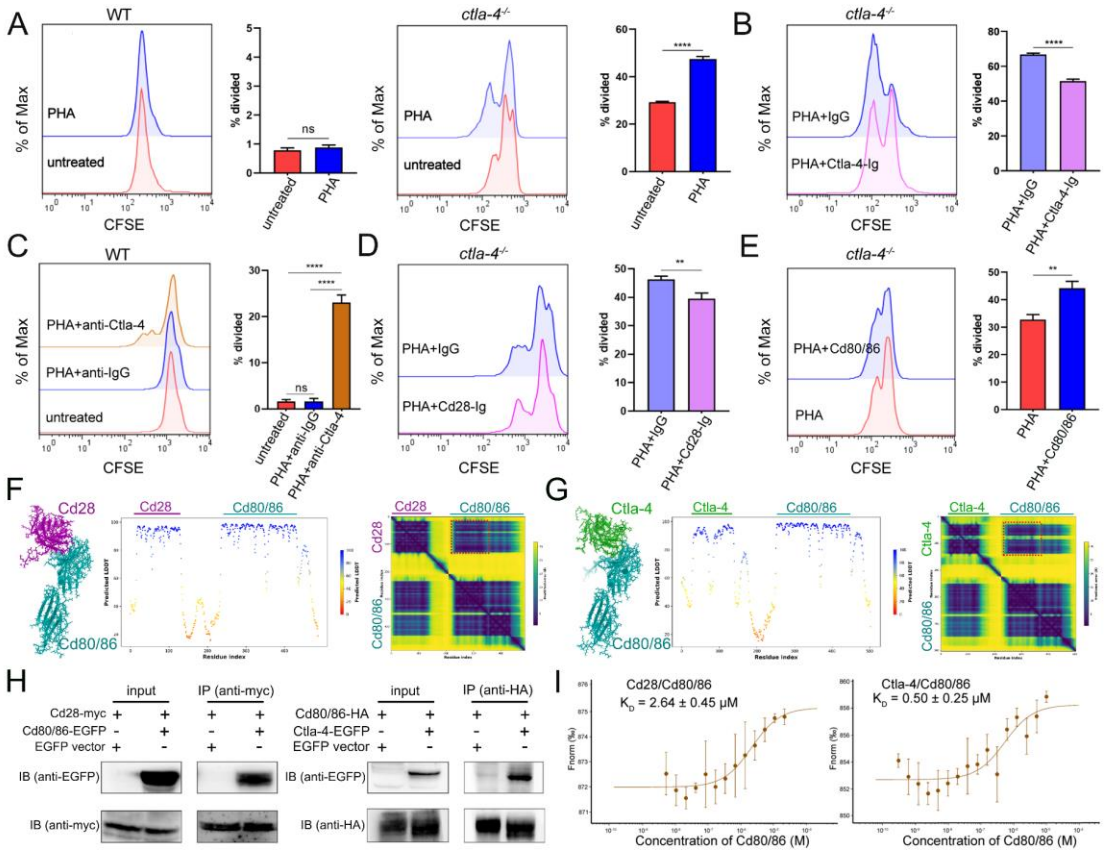

Fig.7 Examination on the inhibitory function of Ctla-4 in T cell activation. **A** Assessment of the proliferative activity of T cells from wild-type and *ctla-4*$^{-/-}$ zebrafish by a mixed lymphocyte reaction combined with PHA-stimulation. The CFSE dilution, which served as an indicator of lymphocyte proliferation, was measured through flow cytometry. **B** Assessment of the proliferative activity of lymphocytes from *ctla-4*$^{-/-}$ zebrafish by the administration of sCtla-4-Ig. **C** Assessment of the proliferative activity of lymphocytes from wild-type zebrafish by supplementing anti-Ctla-4 antibody. **D** Assessment of the proliferative activity of lymphocytes from *ctla-4*$^{-/-}$ zebrafish by the administration of sCd28-4-Ig. **E** Assessment of the proliferative activity of lymphocytes

805 from *ctla-4*$^{-/-}$ zebrafish by the administration of recombinant Cd80/86 protein. **F, G**
806 Interactions between Cd80/86 and Cd28 (**F**), and Cd80/86 and Ctla-4 (**G**) as predicted
807 by AlphaFold2. On the left are structural models depicting Cd80/86 in complex with
808 Cd28 or Ctla-4. The center panels display per-residue model confidence scores (pLDDT)
809 for each structure, using a color gradient from 0 to 100, where higher scores indicate
810 increased confidence. The right panels show the predicated aligned error (PAE) scores
811 for each model. The well-defined interfaces between Cd28 or Ctla-4 and Cd80/86 are
812 highlighted with red dashed squares. **H** The interaction between Cd80/86 and Cd28
813 (left), and Cd80/86 and Ctla-4 (right) were verified by Co-IP. **I** Binding affinities of the
814 Cd80/86 protein for the Cd28 and Ctla-4 proteins were measured by the MST assay.
815 The K_D values are provided. Data are presented as mean ± standard deviation (SD),
816 which were calculated from three independent experiments. Statistical significance was
817 assessed through an unpaired Student's t test ($^{**}p < 0.01$; $^{***}p < 0.001$; ns denotes no
818 statistical significance).

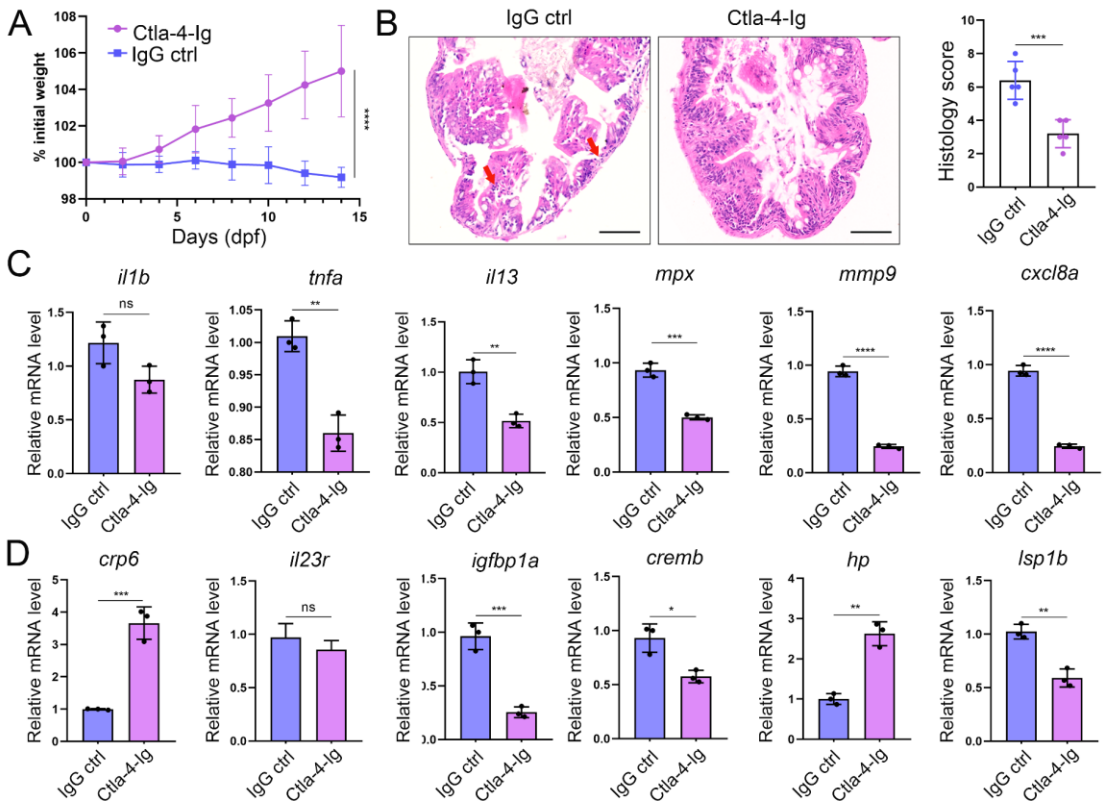

Fig.8 In vivo inhibition of intestinal inflammation by Ctla-4-Ig. **A** Percent initial weight of zebrafish after injection of the Ctla-4-Ig or the IgG isotype control. In each group, n = 6. Data show means with SEM analyzed by two-way ANOVA with Sidak's correction for multiple comparisons. **B** Representative H&E staining analysis of histopathological changes and quantitation of histology score in the posterior intestine from Ctla-4-Ig or IgG isotype control-supplemented *ctla-4*$^{-/-}$ zebrafish. Scale bar: 50 μm. **C** The mRNA expression levels of inflammation-related genes in the Ctla-4-Ig or IgG isotype control treatment groups of *ctla-4*$^{-/-}$ zebrafish. **D** The mRNA expression levels of IBD biomarker genes and IBD-related genes in the Ctla-4-Ig or IgG isotype control treatment groups of *ctla-4*$^{-/-}$ zebrafish. The *p* value was generated by unpaired two-tailed Student's *t-test*. $^{**}p < 0.01$; $^{***}p < 0.001$; $^{****}p < 0.0001$.

Supplemental Figures

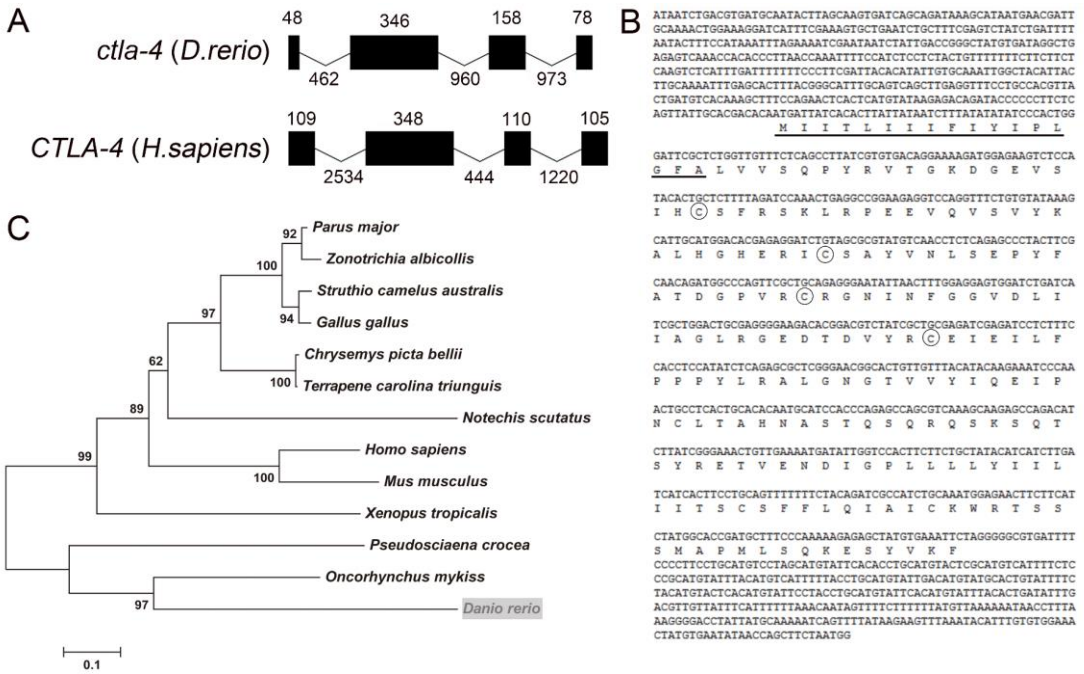

Fig. S1 The organization, sequence and phylogenetic analysis of zebrafish *ctla-4* gene. **A** Comparison of the intron/exon organizations of *ctla-4* gene in zebrafish and humans. Exons and introns are shown with black boxes and lines, and their size are indicated by the numbers found above and below the sequences respectively. **B** The nucleotide and amino acid sequences of *ctla-4* gene and Ctla-4 protein. The underline indicates the signal peptide, the circles represent the conserved cysteine residues. **C** Phylogenetic analysis of the relationship of Ctla-4 between zebrafish and other species. The unrooted phylogenetic tree was constructed through the neighbor-joining method based on the amino acid alignment (ClustalX) of amino acid sequences. The numbers represent the percentage bootstrap confidence derived from 500 replicates.

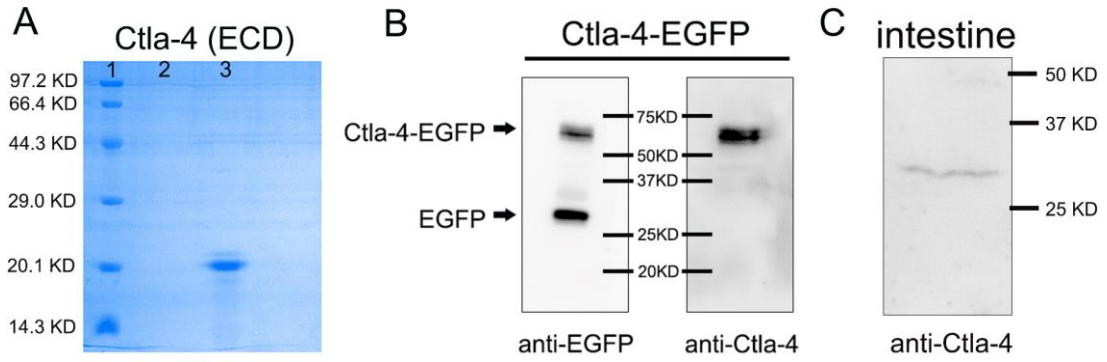

Fig. S2 Preparation of mouse anti-Ctla-4 antibody. **A** SDS-PAGE detection of the recombinant Ctla-4 protein with extracellular domain (ECD). Lane 1, 2 and 3 represent the protein markers, blank, and target protein, respectively. **B** Western blot analysis of the mouse anti-EGFP and anti-Ctla-4 antibodies that bind to the recombinant Ctla-4-EGFP fusion proteins expressed in HEK293T cells. **C** Western blot analysis of native Ctla-4 protein in zebrafish intestinal tissues using mouse anti-Ctla-4 antibody.

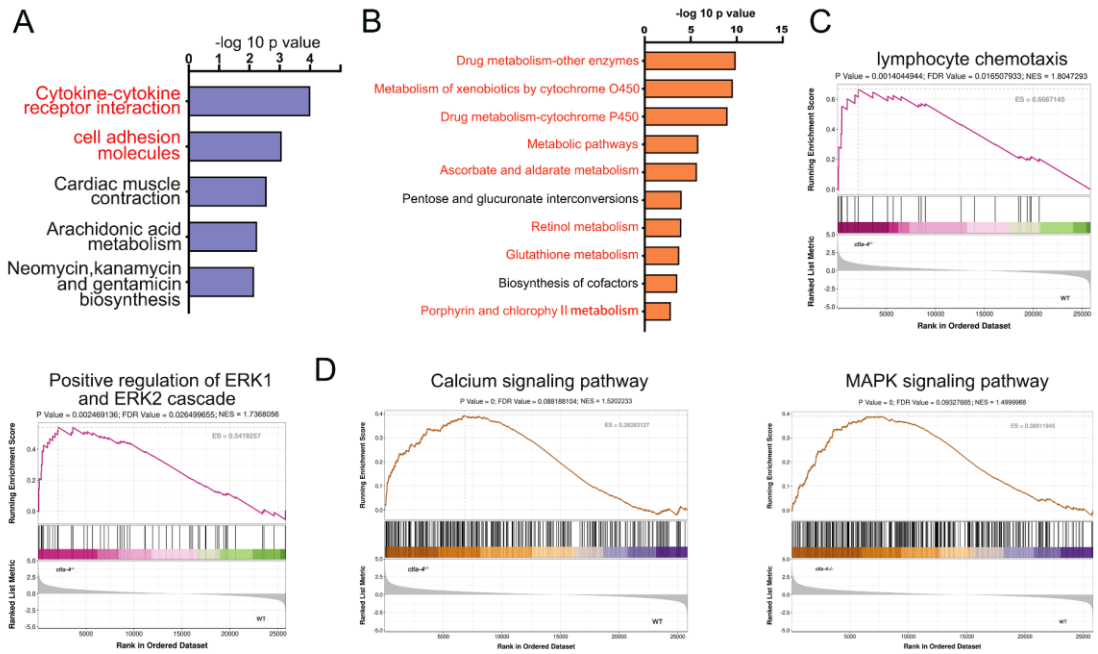

Fig. S3 Examination on the functional genes and pathways associated with the IBD-like phenotype in *ctla-4*$^{-/-}$ zebrafish. **A** Top 5 KEGG enrichment bar plot of up-regulated

genes in *ctla-4*$^{-/-}$ zebrafish intestines versus wild-type zebrafish intestines. **B** Top 10 KEGG enrichment bar plot of down-regulated genes in *ctla-4*$^{-/-}$ zebrafish intestines versus wild-type zebrafish intestines. **C, D** Changes in the expression of genes associated with lymphocyte chemotaxis, positive regulation of ERK1/ERK2 cascades, Calcium and MAPK signaling pathways in the *ctla-4*$^{-/-}$ zebrafish intestines analyzed by using a collection of pre-defined gene sets retrieved from GO (**C**) and KEGG (**D**) database. The *p* value, false discovery rates (FDR) and normalized enrichment score (NES) are shown above each pathway graph.

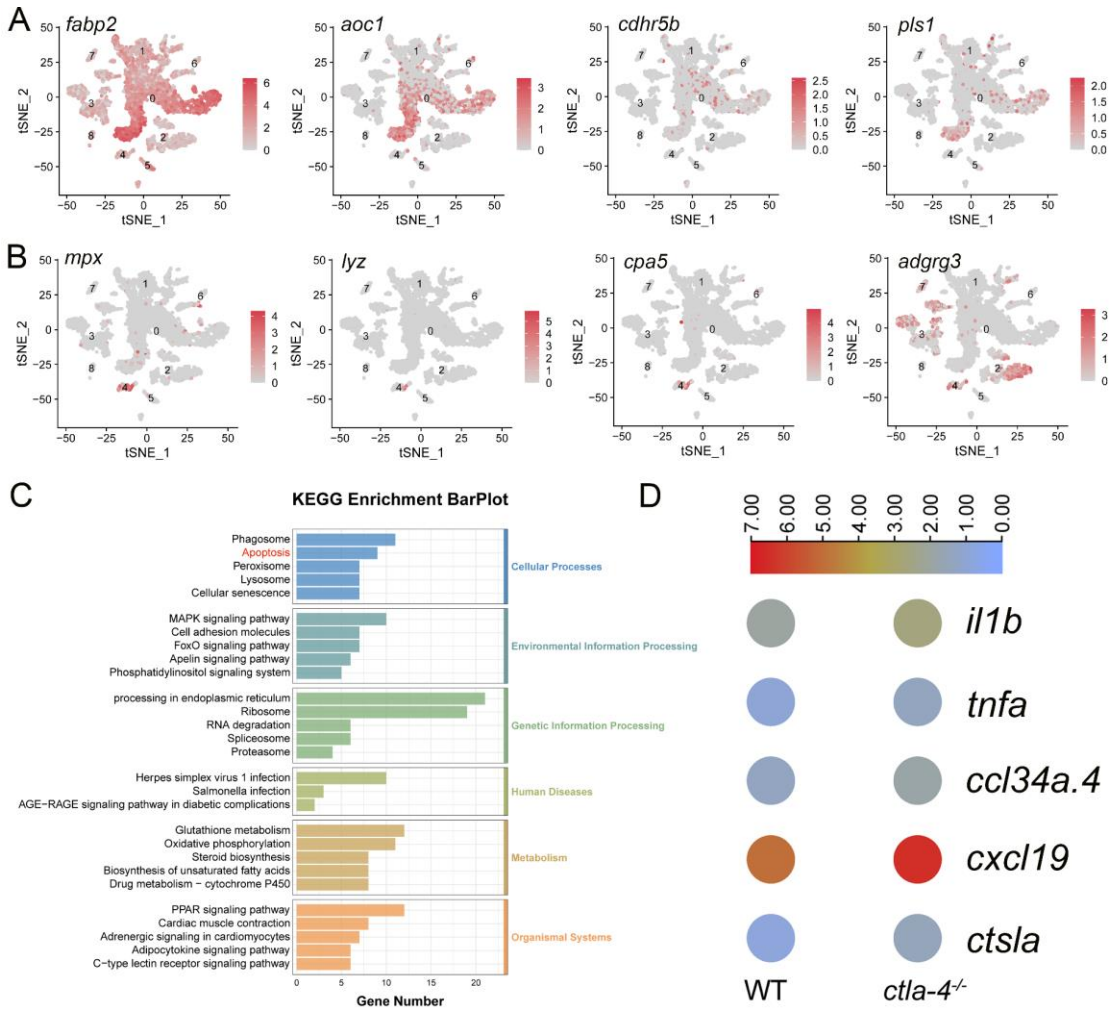

865 **Fig. S4** Examination on the involvement of apoptotic process in epithelial cells and
866 expression of inflammation-related genes in neutrophils and B cells in the intestines of
867 *ctla-4*$^{-/-}$ zebrafish. **A** Expression map of the epithelial markers within the cell
868 populations of the zebrafish intestines. **B** Expression map of the neutrophil markers
869 within the cell populations of the zebrafish intestines. **C** KEGG enrichment bar plot of
870 all DEGs from epithelial cells. **D** Heatmap of inflammation-related genes in B cells
871 from wild-type and *ctla-4*$^{-/-}$ intestines.

872

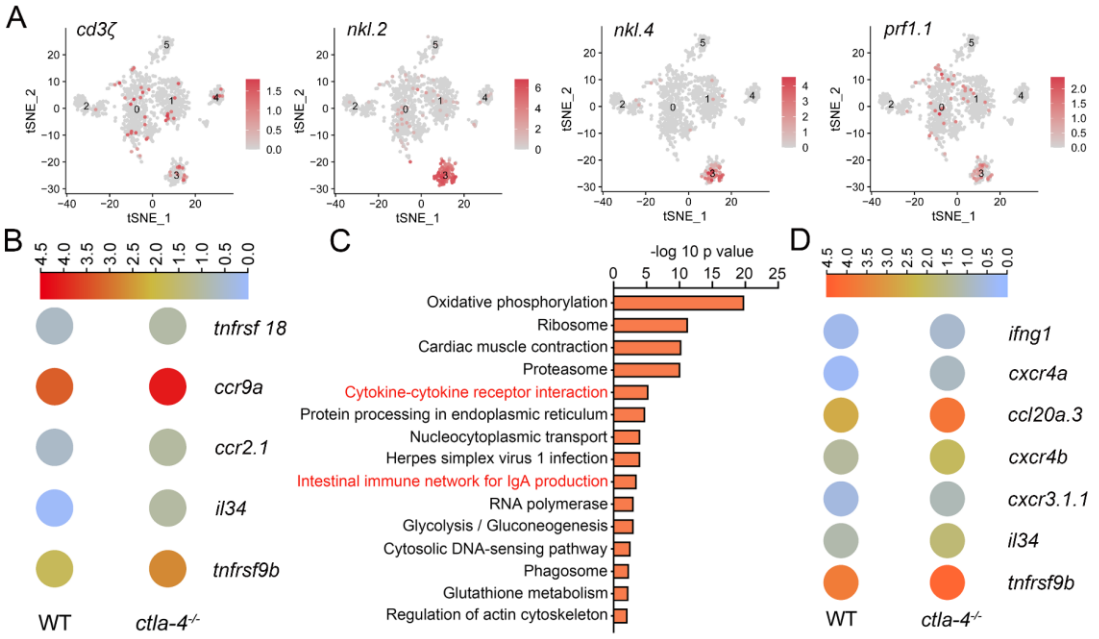

873

874 **Fig. S5** Examination on the activation of T cell subsets in the intestines of *ctla-4*$^{-/-}$
875 zebrafish. **A** Marker gene expression in individual cluster identifying the cluster as
876 NKT cells. **B** Heatmap of up-regulated genes involved in cytokine-cytokine receptor
877 interaction in NKT cells among the wild-type and *ctla-4*$^{-/-}$ samples. **C** KEGG
878 enrichment analysis showing top 15 terms of up-regulated genes in Cd8^{+} T cells in *ctla-*
879 *4*$^{-/-}$ samples versus wild-type samples. **D** Heatmap of up-regulated genes involved in

880 cytokine-cytokine receptor interaction in $Cd8^+$ T cells among the wild-type and *ctla-4*$^{-}$

881 $^{/-}$ samples.

882

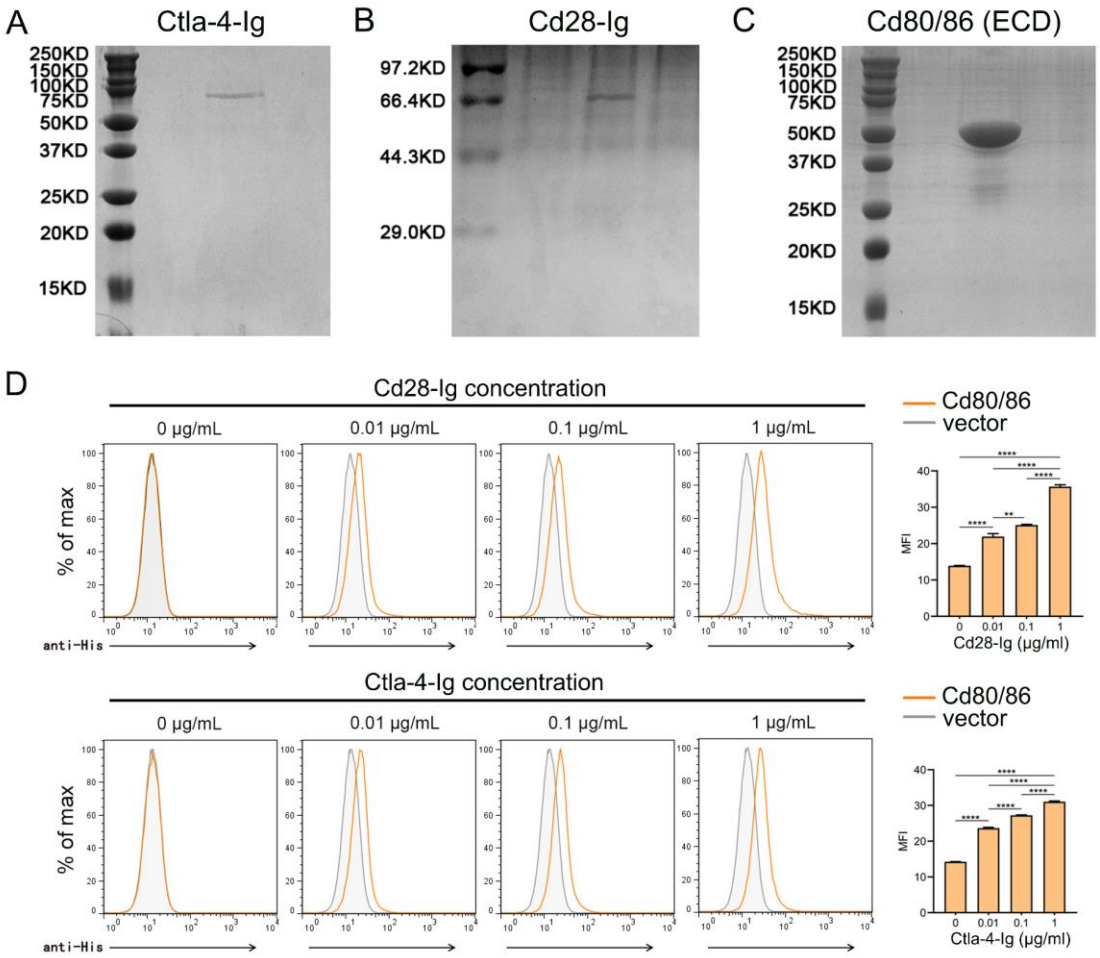

883

884 **Fig. S6** Preparation of recombinant proteins and examination on the molecular

885 interactions. **A-C** SDS-PAGE detection of the purified recombinant soluble Ctla-4-Ig

886 (**A**) and Cd28-Ig (**B**) proteins and the Cd80/86 extracellular domain (ECD) (**C**) with

887 Coomassie brilliant blue staining. **D** Flow cytometry analysis of the interaction between

888 Cd80/86 and Cd28 (up), as well as Cd80/86 and Ctla-4 (down). Data are presented as

889 mean ± SD, which were calculated from three independent experiments. Statistical

890 significance was evaluated using an unpaired Student's t test ($^{**}p < 0.01$; $^{***}p < 0.001$).